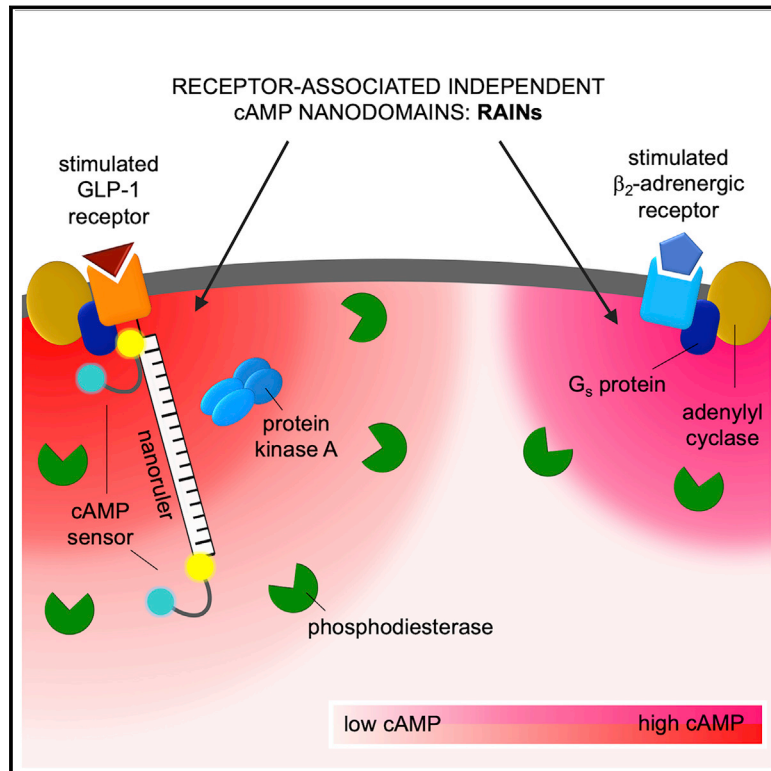


Receptor-associated independent cAMP nanodomains mediate spatiotemporal specificity of GPCR signaling

Graphical abstract



Authors

Selma E. Anton, Charlotte Kayser, Isabella Maiellaro, ..., Martin Falcke, Martin J. Lohse, Andreas Bock

Correspondence

martin.lohse@isarbioscience.de (M.J.L.), andreas.bock@medizin.uni-leipzig.de (A.B.)

In brief

GPCRs signal via localized regions of cAMP that do not mix, leading to action of independent on/off switches rather than coupling via a shared pool of signaling molecules.

Highlights

- Receptors signal via receptor-associated independent cAMP nanodomains (RAINs)
- RAINs constitute entirely self-sufficient, independent cell signaling units
- When receptors are strongly stimulated, RAINs may fuse, and bulk cAMP increases
- Cells may use thousands of independent RAINs to orchestrate signaling specificity

Article

Receptor-associated independent cAMP nanodomains mediate spatiotemporal specificity of GPCR signaling

Selma E. Anton,^{1,2,10} Charlotte Kayser,^{1,10} Isabella Maiellaro,^{2,3,10} Katarina Nemeč,^{1,2} Jan Möller,^{1,2} Andreas Koschinski,⁴ Manuela Zaccolo,⁴ Paolo Annibale,^{1,2,5} Martin Falcke,^{1,6} Martin J. Lohse,^{1,2,7,8,11,12,*} and Andreas Bock^{1,2,9,11,*}

¹Max Delbrück Center for Molecular Medicine in the Helmholtz Association, Robert-Rössle-Strasse 10, 13125 Berlin, Germany

²Institute of Pharmacology and Toxicology, University of Würzburg, Versbacher Str. 9, 97078 Würzburg, Germany

³School of Life Sciences, Department of Neuroscience, University of Nottingham, Nottingham NG7 2UH, UK

⁴Department of Physiology, Anatomy and Genetics, University of Oxford, Parks Road, Oxford OX1 3PT, UK

⁵School of Physics and Astronomy, University of St Andrews, North Haugh, St. Andrews KY16 9SS, UK

⁶Department of Physics, Humboldt University, Newtonstr. 15, 12489 Berlin, Germany

⁷Institute for Chemistry and Biochemistry, Free University Berlin, Takustr. 3, 14195 Berlin, Germany

⁸ISAR Bioscience Institute, Semmelweisstrasse 5, 82152 Planegg, Munich, Germany

⁹Rudolf Boehm Institute of Pharmacology and Toxicology, Medical Faculty, University of Leipzig, Härtelstr. 16-18, 04107 Leipzig, Germany

¹⁰These authors contributed equally

¹¹Senior author

¹²Lead contact

*Correspondence: martin.lohse@isarbioscience.de (M.J.L.), andreas.bock@medizin.uni-leipzig.de (A.B.)

<https://doi.org/10.1016/j.cell.2022.02.011>

SUMMARY

G protein-coupled receptors (GPCRs) relay extracellular stimuli into specific cellular functions. Cells express many different GPCRs, but all these GPCRs signal to only a few second messengers such as cAMP. It is largely unknown how cells distinguish between signals triggered by different GPCRs to orchestrate their complex functions. Here, we demonstrate that individual GPCRs signal via receptor-associated independent cAMP nanodomains (RAINs) that constitute self-sufficient, independent cell signaling units. Low concentrations of glucagon-like peptide 1 (GLP-1) and isoproterenol exclusively generate highly localized cAMP pools around GLP-1- and β_2 -adrenergic receptors, respectively, which are protected from cAMP originating from other receptors and cell compartments. Mapping local cAMP concentrations with engineered GPCR nanorulers reveals gradients over only tens of nanometers that define the size of individual RAINs. The coexistence of many such RAINs allows a single cell to operate thousands of independent cellular signals simultaneously, rather than function as a simple “on/off” switch.

INTRODUCTION

Receptors and their downstream signaling pathways regulate essentially all functions of multicellular organisms. The main class of receptors is constituted by G protein-coupled receptors (GPCRs) and their downstream intracellular second messengers, notably cAMP and calcium (Rosenbaum et al., 2009; Weis and Kobilka, 2018). The human body expresses more than 800 GPCRs (Fredriksson et al., 2003; Hauser et al., 2017; Insel et al., 2015; Sriram and Insel, 2018), and approximately half of these sense extracellular ligands, such as neurotransmitters and hormones. More than 200 GPCRs regulate receptor-specific cell functions primarily through modulation of cAMP (Avet et al., 2020; Inoue et al., 2019; Pándy-Szekeres et al., 2018; Southan et al., 2016).

Since a single cell can express up to 100 different GPCRs (Insel et al., 2015), it poses a formidable challenge for a cell to

distinguish between the inputs from its different GPCRs to assure specific downstream cell functions. This appears particularly difficult for the many GPCRs that stimulate intracellular cAMP, which has been generally considered a highly diffusible molecule that would rapidly equilibrate across a cell and would, thus, produce the same biochemical response irrespective of the specific GPCR.

Attempts to search for specific signaling signatures of different GPCRs have been made for several decades. Thus, it has been shown long ago that in some cells, for example, cardiac myocytes and hepatocytes, two different GPCRs may increase intracellular cAMP levels to the same extent but may have distinct functional effects (Brunton et al., 1979; Buxton and Brunton, 1983; Di Benedetto et al., 2008; Hayes et al., 1979; Hayes et al., 1980; Nikolaev et al., 2010). A classic example is the observation that isoproterenol (via β -adrenergic receptors) and prostaglandin E₁ (via EP

receptors) cause the same cAMP increase, but only isoproterenol increases cardiac contractile force and activates glycogen metabolism (Buxton and Brunton, 1983). Similarly, we have shown that in cardiac myocytes stimulation of β_2 -adrenergic receptors (β_2 -ARs) increases cAMP only locally, whereas stimulation of β_1 -ARs increases cAMP globally, eventually leading to changes in gene transcription (Bathe-Peters et al., 2021; Nikolaev et al., 2006; Nikolaev et al., 2010). Another example suggests that basal cAMP levels at the cell membrane may be higher than in the bulk cytosol and that low concentrations of agonists may be sufficient to trigger responses limited to the cell membrane (Agarwal et al., 2014; Civciristov et al., 2018; Halls and Cooper, 2010; Rich et al., 2000; Rich et al., 2001; Rich et al., 2007). Such studies have given rise to the concept that compartmentation of cAMP signaling may describe the ability of cells to spatially separate different cAMP signals and, consequently, to trigger distinct downstream responses (Langeberg and Scott, 2015; Lefkimiatis and Zaccolo, 2014; Maiellaro et al., 2016; Scott and Pawson, 2009; Surdo et al., 2017; Taylor et al., 2012; Tovey et al., 2008; Wong and Scott, 2004).

For a long time, the concept of compartmentation appeared to be contradicted by observations that cAMP is essentially a freely diffusible second messenger (Agarwal et al., 2016; Bacskai et al., 1993; Chen et al., 1999; Huang and Gillette, 1993; Lohse et al., 2017; Nikolaev et al., 2004; Nikolaev et al., 2006; Richards et al., 2016), which would preclude the formation of intracellular concentration gradients and subcellular compartments. However, recently we have shown that under basal conditions, cAMP is mostly bound to intracellular binding sites and that free diffusion only occurs once its levels are elevated well above the number of its binding sites (Bock et al., 2020). This is supported by the recent discovery of liquid-liquid phase separation of a regulatory protein kinase A subunit (PKA R1 α) that sequesters cAMP (Zhang et al., 2020). We have further shown that this leads to very low concentrations of free cAMP, which in turn allows cAMP phosphodiesterases (PDEs) to generate nanometer-size domains of even lower cAMP, where local cAMP targets are protected from cellular cAMP signals (Bock et al., 2020).

Along these lines, we reasoned that the existence of cAMP binding sites at micromolar concentrations might provide a mechanism to generate and shape cAMP signals triggered by receptor stimulation and might permit the formation of gradients of elevated cAMP concentrations around individual GPCRs. Such spatially limited cAMP gradients might in turn enable cells to specifically sense cAMP signals stemming from a particular GPCR and to propagate GPCR-specific cAMP signals to defined downstream functions.

We therefore set out to search for such domains of high cAMP concentrations associated with GPCRs. To do so, we investigated specifically two G_s -coupled GPCRs: first, the glucagon-like peptide-1 receptor (GLP-1R), a receptor playing a key role in glucose metabolism and in diabetes therapy (Drucker, 2018; Drucker et al., 2017) that responds to peptidic as well as nonpeptidic agonists (Fletcher et al., 2016; Müller et al., 2019; Zhao et al., 2020). GLP-1Rs regulate insulin secretion in pancreatic β -cells via cAMP-dependent stimulation of PKA, and this effect appears to require cellular compartmentation of PKA via anchoring proteins (Lester et al., 1997). In addition, we studied the β_2 -AR,

the main receptor mediating the effects of epinephrine and norepinephrine, which has also been linked to compartment-dependent downstream effects (Buxton and Brunton, 1983; Nikolaev et al., 2006; Nikolaev et al., 2010).

We aimed to explore such domains by fusing a FRET-based cAMP biosensor to receptors with ruler-like spacers of defined nanometer length, to map cAMP levels at defined distances from the receptors. Finally, to show the relevance of such putative domains of high cAMP, we measured activation of downstream PKA with similarly targeted constructs to generate activity maps around individual GPCRs.

RESULTS

To provide direct evidence for the existence of putative cAMP compartments in the vicinity of individual GPCRs, we designed three different FRET-based cAMP biosensors. The first is *GLP1R-camps* that is composed of the human GLP-1R fused to the cAMP biosensor *Epac1-camps* (Nikolaev et al., 2004) (Figure 1) to measure cAMP in the immediate vicinity of the GLP-1R. The second sensor, *Epac1-camps-CAAX*, was used to measure cAMP in the immediate vicinity of the cell membrane. And untargeted *Epac1-camps* served as a sensor for bulk cytosolic cAMP levels (Figure 1A).

The functionality and localization of the sensors were assessed in several control experiments (Figures 1A and S1). We showed that the sensors retained the functionalities of their parent components by demonstrating that (1) the *GLP1R-camps* sensor bound GLP-1-(7-36)-amide (from here on termed GLP-1) and stimulated whole-cell cAMP production with nanomolar potency similar to wild-type GLP-1R (Figure S1A), (2) upon stimulation with GLP-1, single HEK cells transiently expressing *GLP1R-camps* responded with a change in FRET ratio (Figure S1B), (3) this FRET change specifically indicated increases in cAMP, since a mutated construct *GLP1R-camps-R279E*, which does not bind cAMP, showed no FRET change in response to a variety of cAMP-increasing stimuli (Figure S1C), and (4) all three sensors (*GLP1R-camps*, *Epac1-camps-CAAX*, and *Epac1-camps*) had the same affinity for cAMP (Figure S1D). Finally, we confirmed that the three sensors displayed the expected subcellular distribution when expressed in HEK cells: confocal microscopy showed that the *GLP1R-camps* and *Epac1-camps-CAAX* were expressed at the cell membrane, while the untargeted *Epac1-camps* showed a ubiquitous cytosolic expression (Figure 1A).

To assess basal cAMP concentrations in the three compartments, we employed a previously developed calibration approach for cAMP determination in intact cells (Börner et al., 2011) (Figure 1B). This approach uses inhibition of basal activity of adenylyl cyclase with MDL-12,330A to reach minimal levels of cAMP (Figure 1B; R_{MIN}). Addition of 100 μM of MDL-12,330A to cells expressing either of the three sensors resulted in quite distinct FRET responses: it strongly decreased cAMP levels at the GLP-1R and at the cell membrane in general (Figure 1C, orange and green traces, respectively), but much less in the bulk cytosol (Figure 1C, blue trace).

Saturation of all sensors was subsequently reached by application of the cell-permeable, specific Epac activator 8-Br-2'-O-Me-cAMP-AM, followed by inhibition of endogenous

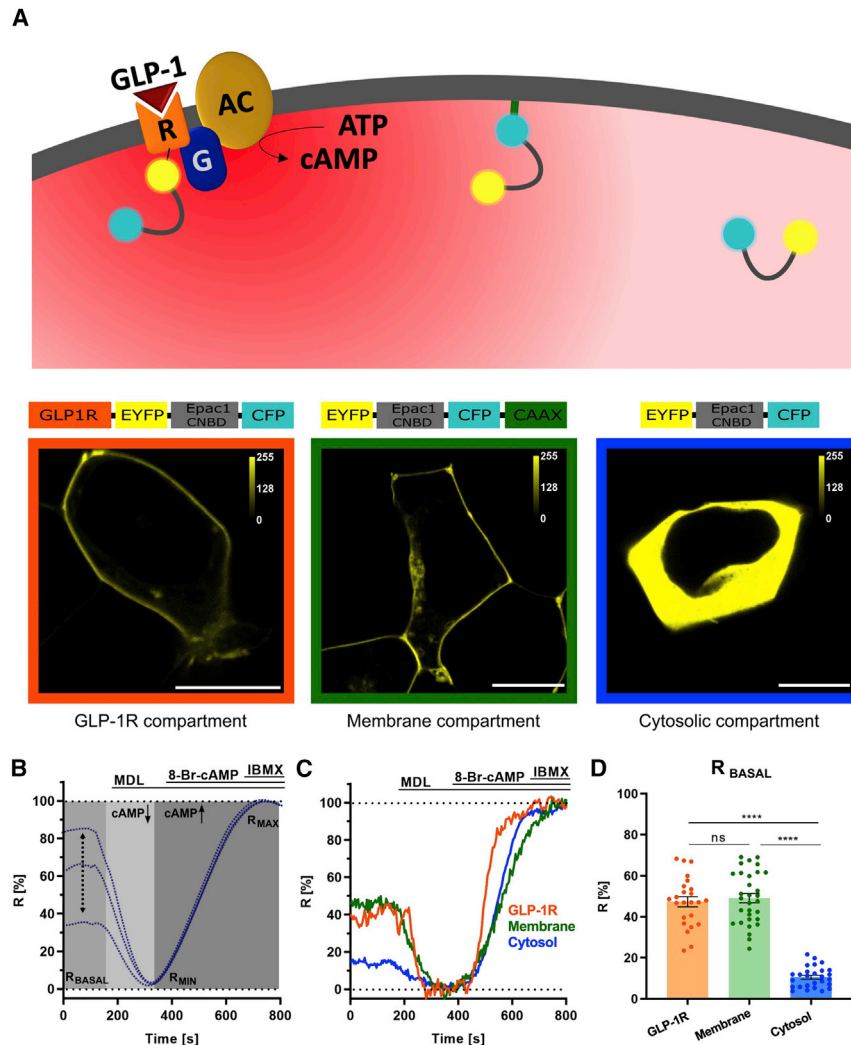


Figure 1. Targeted cAMP reporters reveal GPCR- and membrane-associated cAMP pools

(A) Molecular tools to monitor cAMP in different cellular compartments. Upper: targeting *Epac1-camps* allows measuring cAMP levels in the direct vicinity of the GLP-1R, the cell membrane, and bulk cytosol, respectively. R, GLP-1R; G, stimulatory G protein; AC, adenylyl cyclase. Lower: domain structure and cellular localization of *GLP1R-camps* (orange), *Epac1-camps-CAAX* (green), and *Epac1-camps* (blue). CNBD, cyclic nucleotide-binding domain. Shown are representative confocal images of HEK cells transiently expressing the indicated constructs. Scale bar, 10 μ m.

(B) Experimental approach to assess relative cAMP concentrations. Shown are simulated traces for three different compartments (blue dotted lines). ACs are inhibited by MDL-12,330A (100 μ M) resulting in a decrease of FRET ratio (R_{MIN}). This decrease is dependent on the initial concentration in a compartment (R_{BASAL} , black dotted arrow). Addition of 8-Br-2'-O-Me-cAMP-AM (20 μ M) and IBMX (100 μ M) saturates *Epac1-camps* (R_{MAX}). FRET traces are normalized to R_{MIN} (set to 0%) and R_{MAX} (set to 100%). The basal cAMP level in a compartment is directly given by the intersection with the y axis or calculated as $R_{BASAL} = (R - R_{MIN}) / (R_{MAX} - R_{MIN}) \times 100$.

(C) Representative time courses of changes in FRET ratio of HEK cells expressing *GLP1R-camps* (orange), *Epac1-camps-CAAX* (green), and *Epac1-camps* (blue) following the protocol described in (B). (D) cAMP levels at GLP-1R are higher than in the bulk cytosol. Quantification of basal cAMP signals from experiments as shown in (C). n = 24 (*GLP1R-camps*), n = 31 (*Epac1-camps-CAAX*), and n = 27 (*Epac1-camps*) cells from 8, 8, and 10 independent experiments, respectively. The columns represent means, the vertical bars SEM. ****p < 0.0001, according to one-way analysis of variance (ANOVA) with Tukey's post hoc test; ns, not significantly different.

See also [Figure S1](#).

PDEs with IBMX, yielding FRET values for maximal cAMP signals (Figures 1B and 1C; R_{MAX}). Calculation of relative basal cAMP levels from appropriate calibration curves (Börner et al., 2011) revealed that these levels were similar in the vicinity of GLP-1R and in the membrane compartment (Figure 1D and compare initial values in Figure 1C), which is expected considering that *GLP1R-camps* is exclusively membrane-localized. Interestingly, cAMP levels appeared to be much lower for the cytosolic sensor *Epac1-camps* (Figure 1D). These data indicate that different basal cAMP concentrations may exist in different regions of a cell, with higher concentrations near the cell membrane than in bulk cytosol, confirming earlier notions of such differences (Agarwal et al., 2014; Rich et al., 2000, 2001, 2007).

Low concentrations of GLP-1 exclusively generate a GLP-1R-associated cAMP pool

To assess the cAMP dynamics in the different compartments at equal GLP-1R expression levels, we stimulated HEK cells with

various concentrations of GLP-1 and monitored cAMP in the different compartments. To do so, cells were transfected with *GLP1R-camps* or bicistronic plasmids encoding either GLP-1R WT plus *Epac1-camps-CAAX* or GLP-1R WT plus *Epac1-camps* (Figure 2).

Upon stimulation with GLP-1, single HEK cells transiently expressing *GLP1R-camps* responded with a change in FRET ratio (Figures 2B–2D). Interestingly, low GLP-1 (1 pM)—a concentration that hardly increased bulk cellular cAMP levels (Figure S1A)—led to a robust cAMP increase in the direct vicinity of GLP-1R (Figure 2B, orange). In contrast, 1 pM GLP-1 induced a significantly smaller increase in cAMP at the cell membrane (Figure 2B, green) and—in line with whole-cell cAMP data (Figure S1A)—showed virtually no cAMP increase in the cell cytosol (Figure 2B, blue). As all three sensors (*GLP1R-camps*, *Epac1-camps-CAAX*, and *Epac1-camps*) display the same affinity for cAMP (Figure S1D) and agonist-stimulated FRET responses are independent of sensors' expression levels (Figures S2D

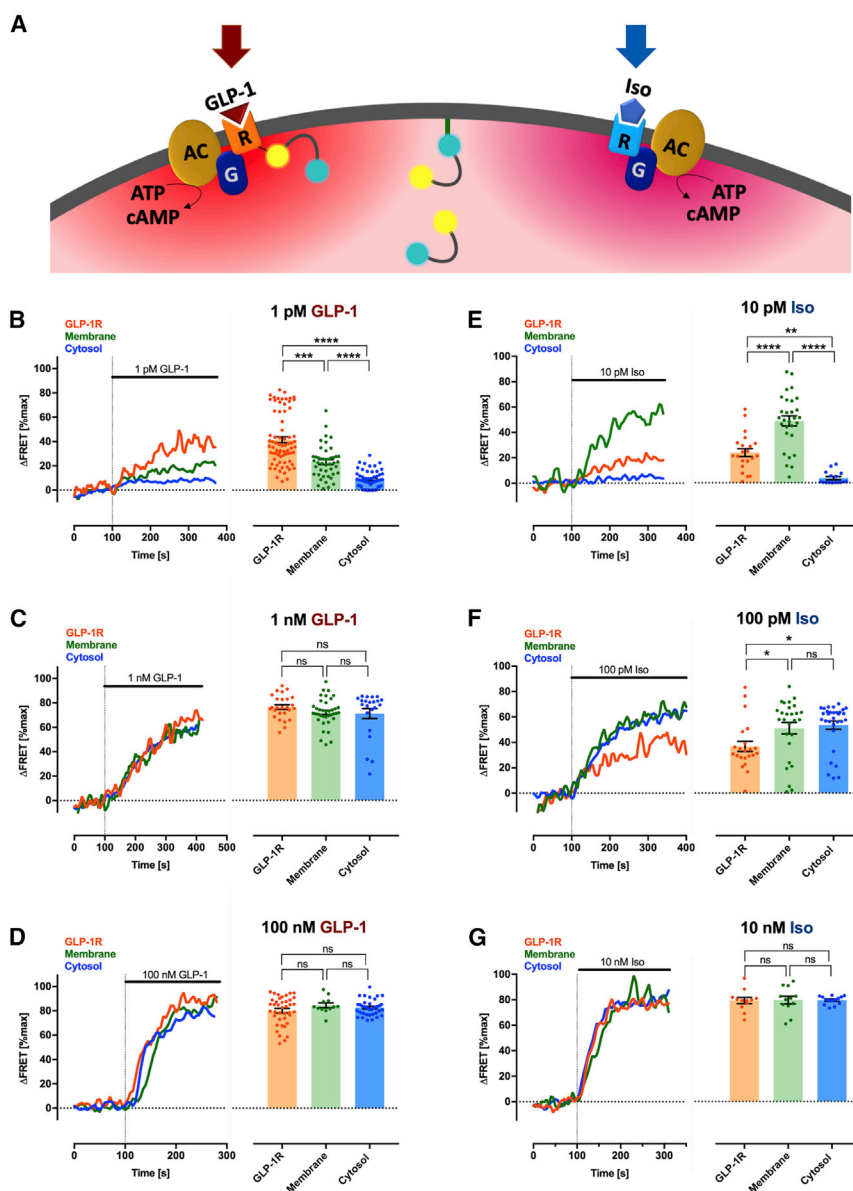


Figure 2. Low concentrations of GLP-1 exclusively generate a GLP-1R-associated cAMP pool that is protected from a foreign GPCR stimulus

(A) *Epac1-camps* is targeted to the GLP-1R (orange R), the cell membrane or the bulk cytosol. cAMP production is triggered by either GLP-1 (B–D) or Iso (E–G) upon activation of GLP-1Rs or endogenous β_2 -ARs (blue R), respectively.

(B–D) Left: representative traces of corrected and normalized FRET ratios (Δ FRET (%max)) in HEK cells transfected with targeted *Epac1-camps* and treated with 1 pM (B), 1 nM (C), or 100 nM GLP-1 (D). Right: normalized, GLP-1-induced FRET ratios pooled from cells measured as in (B–D). The y axis (not shown for clarity) is the same as for the traces on the left. FRET traces are normalized to baseline (set to 0%) and maximal stimulation upon FSK (10 μ M)/IBMX (100 μ M) treatment (set to 100%). (B) n = 74 (*GLP1R-camps*, orange), n = 45 (GLP-1R + *Epac1-camps-CAAX*, green), and n = 55 (GLP-1R + *Epac1-camps*, blue) cells from 18, 11, and 8 independent experiments, respectively; (C) n = 26 (*GLP1R-camps*), n = 38 (GLP-1R + *Epac1-camps-CAAX*), n = 22 (GLP-1R + *Epac1-camps*) cells from 5, 12, and 3 independent experiments, respectively; (D) n = 40 (*GLP1R-camps*), n = 12 (GLP-1R + *Epac1-camps-CAAX*), and n = 37 (GLP-1R + *Epac1-camps*) cells from 9, 4, and 7 independent experiments, respectively.

(E–G) Left: representative traces of corrected and normalized FRET ratios (Δ FRET (%max)) in HEK cells transfected with the respective targeted *Epac1-camps* sensors and treated with 10 pM (E), 100 pM (F), or 10 nM (G) Iso. Right: normalized, Iso-induced FRET ratios pooled from the cells measured as in (E–G). The y axis (not shown for clarity) is the same as for the traces on the left. FRET traces are normalized to baseline (set to 0%) and maximal stimulation upon FSK (10 μ M)/IBMX (100 μ M) treatment (set to 100%). (E) n = 22 (*GLP1R-camps*), n = 29 (GLP-1R + *Epac1-camps-CAAX*), and n = 16 (GLP-1R + *Epac1-camps*) cells from 6, 7, and 3 independent experiments, respectively; (F) n = 22 (*GLP1R-camps*), n = 27 (GLP-1R + *Epac1-camps-CAAX*), and n = 31 (GLP-1R + *Epac1-camps*) cells from 4, 7, and 6 independent experiments, respectively; (G) n = 12 (*GLP1R-camps*), n = 12 (GLP-1R + *Epac1-camps-CAAX*), and n = 14 (GLP-1R + *Epac1-camps*) cells from 3, 4, and 3 independent experiments, respectively.

(B–G) The columns represent means, the vertical bars SEM. ****p < 0.0001, ***p < 0.001, **p < 0.01, *p < 0.05 according to one-way analysis of variance (ANOVA) with Tukey's posthoc test (D,E,G), and according to a Kruskal-Wallis test (B,C,F); ns, not significantly different. See also [Figure S2](#).

and S2E), these data demonstrate that low concentrations of GLP-1 produce a local cAMP pool, which appears to be confined to the immediate vicinity of GLP-1 receptors and spatially distinct from other compartments of the cell. In addition, kinetic analysis indicated that cAMP concentrations increase faster directly at GLP-1 receptors than in the cell cytosol (Figures S2A–S2C).

Elevated GLP-1 concentrations (1 and 100 nM) saturated cAMP levels at the GLP-1R, the cell membrane, and in the cytosol and thereby, abolished these cAMP gradients (Figures 2C and 2D).

The GLP-1R-associated cAMP pool is protected from a foreign GPCR stimulus

Our experiments show that stimulation of *GLP1R-camps* with its cognate agonist GLP-1 produces a receptor-associated cAMP pool, which, at low agonist concentrations, does not appear to spread to other cellular compartments on the timescale of our measurements (i.e., minutes) (Figures 2B–2D). Thus, cAMP that is produced *inside* this receptor-associated compartment is severely hindered in its ability to diffuse *out* of this compartment. We hypothesized that, reciprocally, cAMP from *outside* sources might be restricted in its ability to diffuse *into* the GLP-1

receptor-associated compartment. To provide experimental evidence for this hypothesis, we stimulated endogenous β_2 -ARs with the synthetic agonist isoproterenol (Iso) and measured cAMP within the GLP-1R-associated compartment using *GLP1R-camps* (Figures 2E–2G). Again, we used *Epac1-camps-CAAX* to measure cAMP at the cell membrane and untethered *Epac1-camps* to determine bulk cytosolic cAMP.

Stimulation of β_2 -ARs with low concentrations of Iso (10 pM) strongly increased cAMP levels at the cell membrane; however, the cAMP levels in the GLP-1R-associated compartment were significantly lower, and cytosolic cAMP remained unchanged (Figure 2E). Addition of 100 pM Iso caused a large cAMP response both at the cell membrane and in the cytosol. Interestingly, however, the increase in cAMP levels in the GLP-1R-associated compartment remained significantly lower (Figure 2F). Higher Iso concentrations (10 nM) led to the same relative cAMP increase in all three compartments and thus dissipated the observed cAMP gradients (Figure 2G). Our data suggest that, similar to GLP-1Rs, stimulation of β_2 -ARs produced at least three spatially segregated pools of cAMP. However, the order in which these compartments show increases in cAMP is different: first, cAMP levels increase at the cell membrane, then in the bulk cytosol, and finally in the GLP-1R-associated compartment. These findings contrast with those measured upon GLP-1R stimulation, in which we first observed an increase in the GLP-1R-associated compartment, then at the cell membrane, and finally in the cytosol (Figures 2B–2D).

Together, these data strongly argue for the existence of distinct receptor-associated cAMP pools within a single cell that are spatially segregated and under the control of individual GPCRs. Stimulation of a given receptor would thereby increase cAMP initially in its own immediate compartment (and not affect the compartments of other receptors), followed by an increase of cAMP in the cell membrane compartment and finally, in the cytosol. Importantly, at low GLP-1 concentrations, cAMP gradients remain stable (i.e., the concentrations remain highest at the receptor), and cAMP levels between different compartments do not equilibrate.

Optical mapping of GLP-1R-associated cAMP pools reveals nanometer-size domains

We hypothesized that the size of receptor-associated compartments needs to be very small for a cell to organize signaling inputs from many GPCRs simultaneously with sufficient spatial separation. To provide direct values for the size of such compartments in intact cells, we set out to precisely map the dimensions of these receptor-associated cAMP compartments. To do so, we developed a set of tools where the *Epac1-camps* sensor is placed at defined distances from the GLP-1R. To achieve these defined distances, we used genetically encodable single-alpha-helical (SAH) domain linkers based on ER/K repeats (Bock et al., 2020; Sivaramakrishnan and Spudich, 2011). SAH linkers have been shown to have a size range in nanometers and a rod-like shape that allows us to position two proteins at defined distances from each other.

Based on such linkers, we generated *GPCR nanorulers* by placing a 30 nm SAH linker (SAH30) derived from a Kelch-motif family protein from *Trichomonas vaginalis*, or a tandem spacer

of two such domains, between the GLP-1R and *Epac1-camps* to create *GLP1R-SAH30-camps* or *GLP1R-SAH60-camps*, respectively (Table S1). These constructs should, therefore, measure cAMP levels at 30 or 60 nm distance from the receptor in real time and in intact cells. To verify that the SAH linkers did indeed result in the predicted spacing, we generated a reference construct, which was a membrane-localized version of SAH60 sandwiched between two HaloTags fluorescently labeled with Halo JF-646 (Figure S3A). We performed direct stochastic optical reconstruction microscopy (dSTORM) in fixed cells expressing the labeled construct (Figures 3A and S3). Analysis of the frequency distribution demonstrated that the most abundant molecules had a length of 60 nm (peak of distribution at 69 nm) (Figures S3B and S3C) and, thus, confirmed that an individual SAH30 linker is approximately 30 nm long. Moreover, we confirmed that the *GPCR nanorulers* were expressed at similar expression levels (Figure S3D), had the same potency for stimulating cAMP production as wild-type GLP-1R (Figure S3E), and had the same affinity for cAMP as *Epac1-camps* (Figure S3F).

Stimulation of HEK cells with 1 pM GLP-1—a concentration that robustly increased cAMP within the GLP-1R-associated compartment but virtually not in the cytosol (Figure 2)—led to a significantly smaller relative FRET change in cells expressing *GLP1R-SAH30-camps* compared with *GLP1R-camps* (Figure 3B). As the affinities of the two sensors for cAMP are equal (Figure S3F), these data demonstrate that the cAMP levels at 30 nm distance from the receptor are significantly lower than in its direct vicinity (Figures 3B and 3E). However, the cAMP concentrations measured with *GLP1R-SAH30-camps* were significantly higher than in the cell cytosol (Figures 3B and 3E), suggesting that the GLP-1R-associated cAMP compartment has a dimension of more than 30 nm.

To measure cAMP beyond the 30 nm distance, we stimulated HEK cells expressing the longer *GLP1R-SAH60-camps* nanoruler with 1 pM GLP-1. This resulted in significantly smaller relative FRET changes than those seen with *GLP1R-SAH30-camps* and *GLP1R-camps* (Figures 3B and 3E) and which were only slightly, albeit significantly, larger than the signals measured in the cytosol (Figures 3B and 3E). This suggests that the GLP-1R-associated cAMP pool has a diameter of approximately 60 nm. Given the dimensions of these receptor-associated cAMP pools, we propose to term them *receptor-associated independent cAMP nanodomains* (RAINs).

To assess how these domains change upon stronger stimulation of the receptors, we performed similar experiments with 1 nM GLP-1 (Figure 3C). Interestingly, at these higher concentrations, differences in FRET ratios at 0, 30, and 60 nm distance from the receptor were no longer visible, indicating that the cAMP gradients seen with 1 pM GLP-1 were abolished (Figures 3C and 3F).

As the GLP-1 RAINs are protected from cAMP generated by β_2 -ARs (Figure 2E), we wondered whether the *GLP1R nanorulers*, i.e., *GLP1R-SAH60-camps* and *GLP1R-SAH30-camps*, would sense this “foreign” cAMP earlier than *GLP1R-camps*. To test this hypothesis, we expressed all three constructs at similar levels and stimulated endogenous β_2 -AR in HEK cells with 10 pM Iso (Figure 3D). In line with our hypothesis, *GLP1R-SAH60-camps* detected a significantly larger cAMP increase

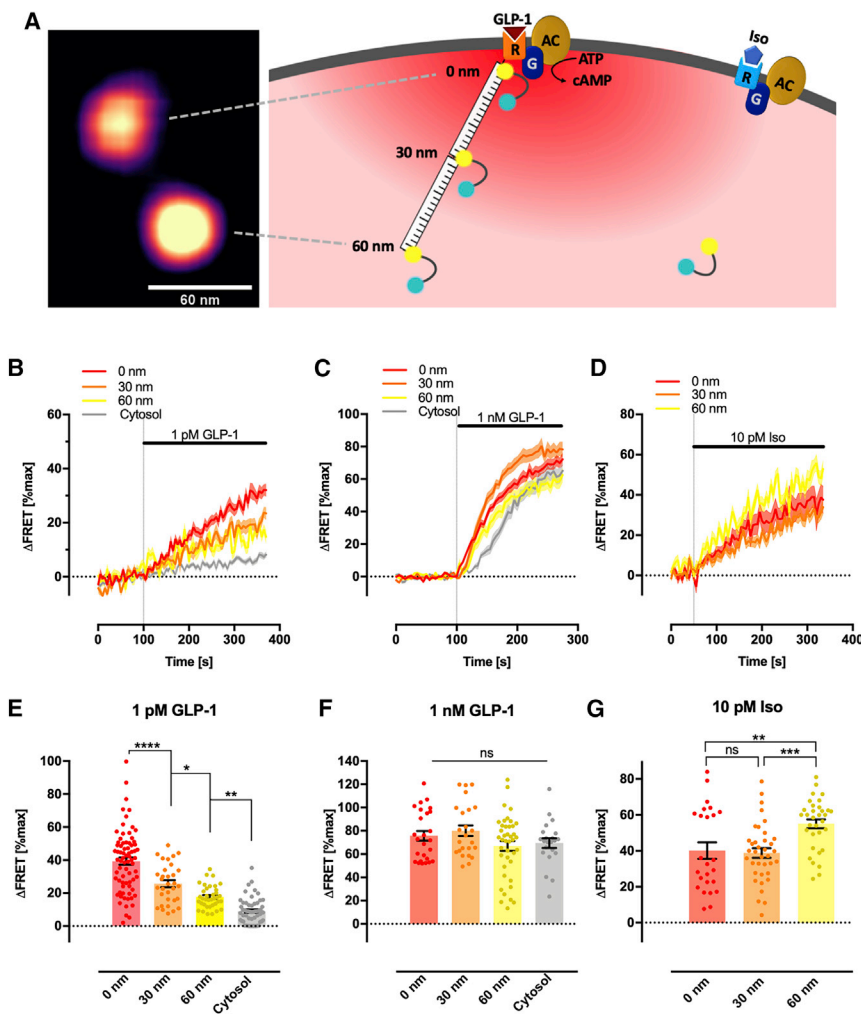


Figure 3. Optical mapping of GLP-1R-associated cAMP pools reveals nanometer-size domains

(A) Genetic incorporation of SAH linkers into *GLP1R-camps* allows optical mapping of local cAMP pools at nanometer distances from the receptor. The length of the SAH60 linker was determined by dSTORM (Figure S3). The dSTORM image on the left shows a membrane-bound SAH60 linker molecule flanked by two labeled Halo tags.

(B, C, E, and F) Mapping of the GLP-1R-associated cAMP pool. (B and C) Averaged traces of corrected and normalized FRET ratios (Δ FRET (%max)) of HEK cells transfected with *GLP1R-camps* (0 nm linker, red), *GLP1R-SAH30-camps* (30 nm linker, orange), *GLP1R-SAH60-camps* (60 nm linker, yellow), or *GLP-1R + Epac1-camps* (cytosol, gray) treated with 1 pM (B) or 1 nM (C) GLP-1 under basal (i.e., PDEs intact) conditions. FRET traces from each individual cell were normalized to baseline (set to 0%) and the averaged maximal stimulation upon FSK (10 μ M)/IBMX (100 μ M) treatment (average set to 100%). Solid lines indicate the mean, shaded areas SEM. (E, F) Normalized, GLP-1-induced FRET ratios from the cells measured: (B) 1 pM GLP-1: n = 74 (0 nm linker), n = 32 (30 nm linker), n = 37 (60 nm linker), n = 55 (cytosol) cells from 18, 8, 12, and 8 independent experiments, respectively, (C) 1 nM GLP-1: n = 26 (0 nm linker), n = 24 (30 nm linker), n = 41 (60 nm linker), and n = 22 (cytosol) cells from 5, 5, 9, and 3 independent experiments, respectively.

(D and G) Mapping of spatial protection of the GLP-1R-associated cAMP pool from a foreign GPCR stimulus. (D) Averaged traces of corrected and normalized FRET ratios (Δ FRET (%max)) in HEK cells transfected with *GLP1R-camps* (0 nm linker, red), *GLP1R-SAH30-camps* (30 nm linker, orange), or *GLP1R-SAH60-camps* (60 nm linker, yellow) stimulated with 10 pM Iso. FRET traces from each individual cell were normalized to baseline (0%) and maximal stimulation upon FSK (10 μ M)/IBMX

(100 μ M) treatment (set to 100%). Solid lines indicate the mean, shaded areas SEM. (G) Normalized, Iso-induced FRET ratios from n = 25 (0 nm linker), n = 37 (30 nm linker), and n = 33 (60 nm linker) cells from 5, 8, and 7 independent experiments, respectively.

(E–G) The columns represent means, the vertical bars SEM. ****p < 0.0001, ***p < 0.001, **p < 0.01, *p < 0.05 according to one-way analysis of variance (ANOVA) with Tukey's post hoc test; ns, not significantly different.

See also Figure S3.

than *GLP1R-SAH30-camps* and *GLP1R-camps* did (Figures 3D and 3G). These data demonstrate that GLP-1R cAMP nanodomains are gradually protected from cAMP generated by other receptors and, thus, further support the existence and size of RAINs.

Localized PDE activity shapes the size of GLP-1R-associated cAMP nanodomains

PDEs have repeatedly been suggested to contribute to the compartmentation of cAMP (Baillie, 2009; Baillie et al., 2019; Bender and Beavo, 2006; Fischmeister et al., 2006; Houslay, 2010; Stangherlin and Zaccolo, 2012). We have demonstrated recently that this is due to the fact that under basal physiological conditions, most cAMP is not freely diffusible but bound to specific sites, which results in free cAMP low enough for individual PDEs to shape cAMP concentration gradients (Bock et al.,

2020). Therefore, we tested whether endogenous PDEs might have a role in shaping RAINs. Pretreatment with the global PDE inhibitor IBMX (100 μ M) alone led to different FRET changes in the direct vicinity of the GLP-1R and at 30 and 60 nm distances from the receptors. This suggests that PDE activity may have different consequences at certain nanometer distances from the receptor (Figures 4A and 4B). Interestingly, IBMX pretreatment abolished the differences in cAMP levels directly at the GLP-1R versus at 30 and 60 nm distance upon stimulation with 1 pM GLP-1 (Figure 4C). These data suggest that localized PDE activity is a key factor in shaping the size of RAINs.

GLP-1 receptor nanodomain signaling requires tethered PKA

The observations that cAMP levels are higher in the immediate vicinity of a GPCR and that these domains are somewhat

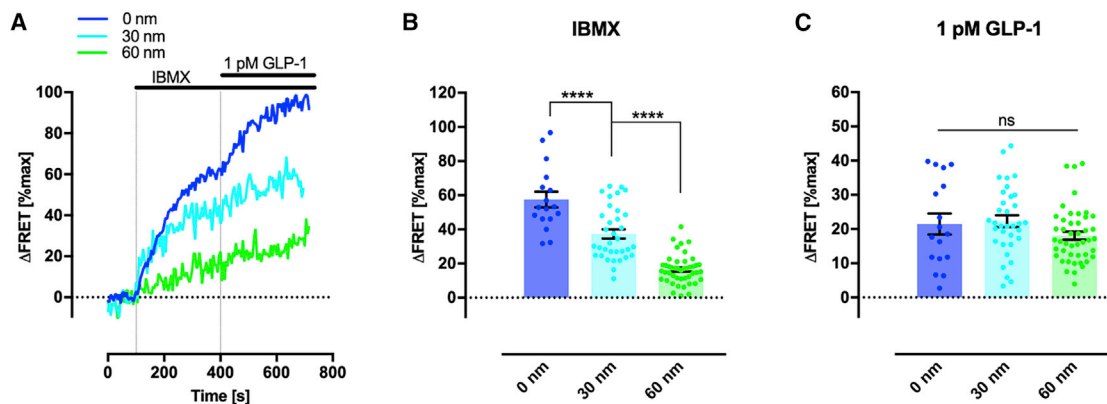


Figure 4. Localized PDE activity shapes the size of GLP-1R-associated cAMP nanodomains

(A) Inhibition of PDE activity differentially increases cAMP levels in the vicinity of GLP-1R and at 30 and 60 nm distance. Shown are representative traces of corrected and normalized FRET ratios (Δ FRET [%max]) in HEK cells transfected with *GLP1R-camps* (0 nm linker, blue), *GLP1R-SAH30-camps* (30 nm linker, turquoise), or *GLP1R-SAH60-camps* (60 nm linker, green) treated sequentially with 100 μ M IBMX and 1 pM GLP-1. FRET traces are normalized to baseline (set to 0%) and the average maximal stimulation upon FSK (10 μ M)/IBMX (100 μ M) treatment (set to 100%). (B and C) Normalized, IBMX- (B) and subsequent GLP-1-induced (C) FRET ratios pooled from all cells measured: $n = 17$ (0 nm linker), $n = 34$ (30 nm linker), and $n = 45$ (60 nm linker) cells from 5, 9, and 12 independent experiments, respectively. The columns represent means, the vertical bars SEM. **** $p < 0.0001$, according to one-way analysis of variance (ANOVA) with Tukey's post hoc test (B), and a Kruskal-Wallis test (C); ns, not significantly different.

protected from the influx of cAMP generated at other receptors can only be explained if cAMP is not freely diffusible at these sites. We have recently discovered that cytosolic cAMP under basal conditions is buffered by binding to specific binding proteins, such as protein kinase A (PKA) (Bock et al., 2020). To assess whether similar mechanisms might account for the formation of cAMP gradients around GPCRs, we investigated whether local cAMP-buffering sites exist within these RAINs. We used the FRET-based PKA activity reporter *AKAR4* (Depry et al., 2011), which reports on endogenous PKA activity upon phosphorylation of its intrinsic PKA substrate. By fusing *AKAR4* to the C terminus of the GLP-1R, we generated the sensor (*GLP1R-AKAR4*) to test for endogenous PKA activity inside RAINs (Figure 5A). We confirmed that *GLP1R-AKAR4* stimulated cAMP production as efficiently as GLP-1 wild-type receptors and that *AKAR4* sensed PKA phosphorylation equally well independent of being tethered to GLP-1R (*GLP1R-AKAR*) or expressed in the cytosol (Figures S4A and S4B). Moreover, confocal microscopy of cells expressing *GLP1R-AKAR4* confirmed that it was appropriately localized at the cell membrane (Figure 5A, left lower panel). As a control for whole-cell PKA activity, we expressed separately but stoichiometrically GLP-1R and *AKAR4*, which leads to whole-cell expression of *AKAR4* (Figure 5A, right lower panel).

Stimulation with 1 pM GLP-1—the concentration that had increased cAMP within the GLP-1R-associated compartment but virtually not in the cytosol (Figure 2)—led to a strong, almost saturating increase in FRET ratio of the *GLP1R-AKAR4* sensor, indicating strong PKA activity inside RAINs (Figure 5B, orange trace). In contrast, the same GLP-1 concentration promoted only very little PKA activity in the cytosol (Figure 5B, blue trace). As before, no such differences were visible at higher GLP-1 concentrations (1 nM); under these conditions, PKA was fully activated both in RAINs and in the cytosol (Figure 5C).

PKA is tethered to molecular signaling complexes by A-kinase-anchoring proteins (AKAPs) (Langeberg and Scott, 2015; Scott and Pawson, 2009; Taylor et al., 2012; Wong and Scott, 2004). This provides a means for cells to localize PKA activity to defined macromolecular signaling complexes at specific cellular locations, thereby exerting spatial control over PKA activity. Strikingly, when HEK cells expressing *GLP1R-AKAR4* were pretreated with St-Ht31, a peptide that disrupts protein-protein interactions between regulatory subunits of PKA and AKAPs, PKA activity in RAINs was entirely lost even upon stimulation with 1 nM GLP-1 (Figure 5D). Remarkably, disrupting AKAP/PKA interactions had no effect on cytosolic PKA activity under the same stimulation conditions (Figure 5D). As expected, pretreatment with the respective inactive control peptide St-Ht31-P had no effect on PKA activity inside RAINs (Figure 5E). These data unequivocally demonstrate the presence of localized PKA activity that is tethered to RAINs. Moreover, these data suggest that RAINs constitute self-sufficient and independent signaling units in which local generation of cAMP by GLP-1 is directly translated into local PKA activity. Of note, since disruption of PKA tethering completely abolished GLP-1R nanodomain signaling, it is necessary that PKA molecules have to be located *inside* the GLP-1R nanodomain. This indicates that diffusion of other PKA molecules from *outside* into these GLP-1R nanodomains does not occur or, at least, does not promote phosphorylation of PKA substrates tethered to the GLP-1 receptor.

Low concentrations of isoproterenol generate a β_2 -AR-associated cAMP pool

We have shown above that β_2 -AR-mediated cAMP stimulation leads to significantly higher cAMP increases at the cell membrane than in the direct vicinity of GLP-1 receptors (Figure 2E). Furthermore, we have demonstrated that GLP-1Rs are protected in a gradual manner from cAMP generated by β_2 -AR

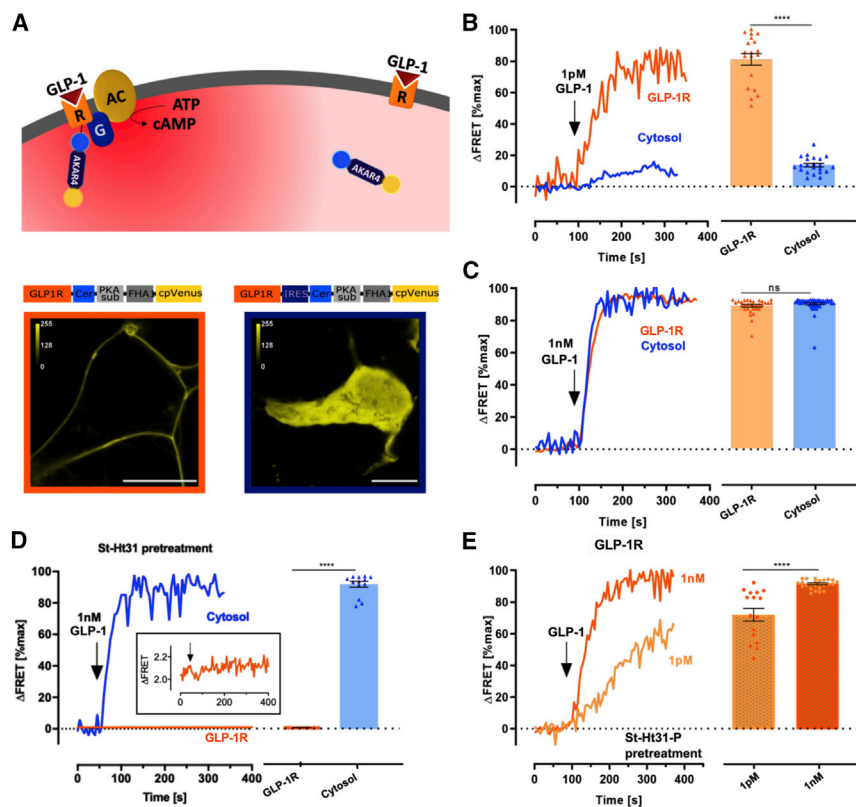


Figure 5. GLP-1R-associated cAMP nanodomain signaling requires tethered PKA

(A) Targeting of A-kinase activity reporter 4 (*AKAR4*) to the GLP-1R or separate stoichiometric expression of cytosolic *AKAR4* and GLP-1R allows measuring local and global cytosolic PKA phosphorylation upon GLP-1R activation, respectively. Domain structures and cellular localization of *GLP1R-AKAR4* (lower left panel) and GLP-1R + *AKAR4* (via transfection of *GLP1R-IRES2-AKAR4*, lower right panel). Shown are representative confocal images of HEK cells transiently expressing the indicated constructs. Scale bar, 10 μ m.

(B and C) Representative traces of corrected and normalized FRET ratios (Δ FRET [%max]) in HEK cells transfected with *GLP1R-AKAR4* (orange) and *GLP1R-IRES2-AKAR4* (blue) and treated with 1 pM (B) or 1 nM (C) GLP-1. FRET traces are normalized to baseline (set to 0%) and maximal stimulation upon FSK (10 μ M)/IBMX (100 μ M) treatment (set to 100%). Right: normalized GLP-1-induced FRET ratios indicating GLP-1R nanodomain (orange) or global cytosolic (blue) PKA phosphorylation from all cells; (B) n = 19 (*GLP1R-AKAR4*), n = 22 (GLP-1R + *AKAR4*) cells from 9 and 4 independent experiments, respectively; (C) n = 25 (*GLP1R-AKAR4*), n = 29 (GLP-1R + *AKAR4*) cells from 8 and 4 independent experiments, respectively.

(D and E) Disruption of PKA anchoring completely abolishes GLP-1R-associated cAMP nanodomain signaling. Experiments were done exactly as in (B and C) upon pretreatment (30 min) with St-Ht31 (100 μ M) (D) or control peptide St-Ht31-P (100 μ M) (E).

(E) (D) St-Ht31 pretreatment disrupts PKA anchoring and abolishes GLP-1 receptor nanodomain signaling (orange) while global cytosolic PKA phosphorylation (blue) remains unaffected; n = 30 (*GLP1R-AKAR4*), n = 14 (GLP-1R + *AKAR4*) cells from 9 and 6 independent experiments, respectively. The inset shows original, non-normalized Δ FRET values and further illustrates the lack of response at *GLP1R-camps*. (E) St-Ht31-P pretreatment does not affect concentration-dependent, GLP-1-stimulated nanodomain PKA phosphorylation; n = 16 (1 pM), n = 27 (1 nM) cells from 9 and 6 independent experiments, respectively. The columns represent means, the vertical bars SEM. ****p < 0.0001, according to an unpaired t test; ns, not significantly different.

See also Figure S4.

activation (Figures 3D and 3G). These data suggest that β_2 -ARs may, in analogy to GLP-1Rs, also generate cAMP nanodomains.

To provide direct evidence for RAINs at β_2 -AR, we designed and cloned *β_2 AR-camps*, a biosensor consisting of the human wild-type β_2 -AR fused to *Epac1-camps* (Figure 6). *β_2 AR-camps* functions like wild-type β_2 -AR with respect to cAMP production (Figure S5A) and shows correct membrane localization (Figure 6B). Stimulation of HEK-AD cells that expressed *β_2 AR-camps* or a bicistronic plasmid encoding β_2 -AR plus *Epac1-camps-CAAX* or *Epac1-camps* at similar expression levels (Figure S5B), with very low concentrations of Iso (1 pM) led to significantly larger cAMP increases at the β_2 -AR and at the cell membrane than in the cytosol (Figure 6C). In contrast to GLP-1Rs, we did not observe differences in the cAMP levels at the β_2 -AR and the cell membrane, which is presumably due to the fact that the endogenous β_2 -ARs expressed in HEK cells (albeit at much lower levels) lead to cAMP elevations in the entire membrane compartment (Figure 6C). At higher concentrations of Iso (10 pM), cAMP nanodomains are maintained, but cAMP levels increase in all compartments, which may indicate the beginning of cAMP nanodomain dissipation (Figure 6D).

Taken together, these data demonstrate that also β_2 -ARs form RAINs, which suggests that RAINs may be a general phenomenon of GPCRs.

Quantitative aspects of RAINs

We have shown that GPCRs generate RAINs that stretch over several tens of nanometers and are protected from cAMP influxes produced by different GPCRs. The differences in cAMP concentrations in different compartments (Figure 2) and at nanometer distances from the receptor at steady state (Figure 3B) are remarkable. We were wondering how these cAMP concentration profiles may be described in quantitative terms.

In the absence of any mechanism that restricts cAMP diffusion dynamics, the cAMP concentration profiles would be dictated by free diffusion and, thus, of hyperbolic nature. At low agonist occupancies (i.e., 1 pM GLP-1), one can assume that the distance between individual, ligand-bound receptors is much larger than the radius of RAINs, and, thus, at 1 pM GLP-1 stimulation, we consider isolated cAMP concentration profiles under the control of a single active GLP-1R (Methods S1; for graphical illustration, see Figure 7). Assuming a constant cAMP diffusion coefficient within RAINs and constant PDE activity in the cytosol,

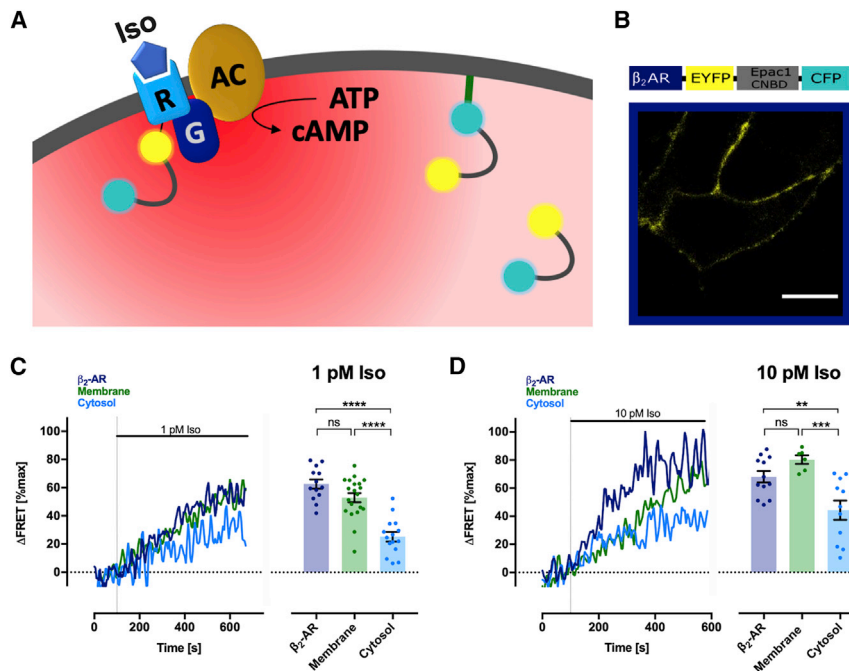


Figure 6. Low concentration of isoproterenol generates a β_2 -AR-associated cAMP pool

(A) *Epac1-camps* is targeted to the β_2 -AR, the cell membrane, or the bulk cytosol. Production of cAMP is triggered by Iso.

(B) Domain structure and cellular localization of β_2 -AR-*camps*. Shown is a representative confocal image of HEK-AD cells transiently expressing β_2 -AR-*camps*. Scale bar, 10 μ m.

(C and D) Left: representative traces of corrected and normalized FRET ratios (Δ FRET (%max)) in HEK-AD cells transfected with targeted *Epac1-camps* and treated with 1 pM (C) or 10 pM (D) Iso. FRET traces are normalized to baseline (set to 0%) and maximal stimulation upon FSK (10 μ M)/IBMX (100 μ M) treatment (set to 100%). Right (same y axis as for FRET traces on the left): normalized, Iso-induced FRET ratios from cells measured as in (C and D). (C) $n = 13$ (β_2 -AR-*camps*), $n = 20$ (β_2 -AR + *Epac1-camps*-CAAX), and $n = 15$ (β_2 -AR + *Epac1-camps*) cells from 5, 6, and 5 independent experiments, respectively. (D) $n = 12$ (β_2 -AR-*camps*), $n = 6$ (β_2 -AR + *Epac1-camps*-CAAX), and $n = 11$ (β_2 -AR + *Epac1-camps*) cells from 5, 3, and 4 independent experiments, respectively. (C and D) The columns represent means, the vertical bars SEM. **** $p < 0.0001$, *** $p < 0.001$, ** $p < 0.01$ according to one-way analysis of variance (ANOVA) with Tukey's post hoc test; ns, not significantly different. See also Figure S5.

the solution of the stationary reaction-diffusion equation (Methods S1 for delineation of formulas [Bentele and Falcke, 2007; Martiel and Goldbeter, 1987; Violin et al., 2008]) indicates that increases of cAMP concentrations in the direct vicinity of receptors should dissipate away from the receptors according to a simple $1/r$ dependency until they reach the cAMP levels of the bulk cytosol.

Based on the data in Figures 3B and 3E, we calculated the increases in cAMP concentrations at the GLP-1R, at 30 and 60 nm distance and in the bulk cytosol upon stimulation with 1 pM GLP-1 (Figure 7B, magenta). Fitting cAMP levels at the receptor and the cytosol (Equation 1 in STAR Methods) strikingly revealed that cAMP concentrations at 30 nm distance (and less so at 60 nm distance) from the receptor are much higher than predicted from a $1/r$ dependency and thereby cannot be explained by simple diffusion and constant cytosolic PDE activities alone (Figure 7B; Methods S1).

At higher agonist concentrations (i.e., 1 nM GLP-1, Figures 3C and 3F), cAMP increases much more at both 30 and 60 nm distances, and cAMP nanodomains appear to broaden (note that at 1 nM GLP-1 Δ [cAMP] is equal at GLP-1R and at 30-nm distance, Figure 7B, blue). Given the much higher receptor occupancy at this agonist concentration and, therefore, a reduced distance between individual active receptors, isolated cAMP concentration profiles can no longer be assumed; instead, the concentration profiles are expected to become more complex in this situation (cf. Equation 2 in Methods S1). In any case, also at high GLP-1 concentrations, it is obvious that increases in cAMP at the receptor do not get smaller in space as would be ex-

pected for simple diffusion and constant cytosolic PDE activities (Figure 7B).

Thus, at both low and high agonist concentrations, our data are not compatible with a simple diffusion model for cAMP but instead would be in line with buffered diffusion of cAMP (Bock et al., 2020), along with cAMP trapping by local molecular crowding or formation of biomolecular condensates (Zhang et al., 2020). Together with differentially localized PDE activity, these mechanisms appear to allow the formation of RAINs where very local effects of cAMP occur. Figure 7B shows that these RAINs broaden at higher agonist concentrations and ultimately dissipate to lead to increases in bulk cytosolic cAMP, which stimulates cAMP effects throughout a cell.

DISCUSSION

Mapping cAMP gradients around individual GPCRs, we have identified RAINs in intact cells. Low agonist concentrations produce a localized receptor-associated cAMP pool that extends up to 60 nm from the receptor. This cAMP pool directly translates into localized, receptor-associated PKA activity and, hence, constitutes a self-sufficient and independent signaling unit. The required presence of PKA regulatory subunits inside RAINs suggests the requirement for localized binding and buffering of cAMP, which would keep the cAMP local and, moreover, enables localized PDEs to shape the size of GPCR-associated independent cAMP nanodomains. Experiments with the β_2 -AR showed similar localized cAMP responses to low levels of

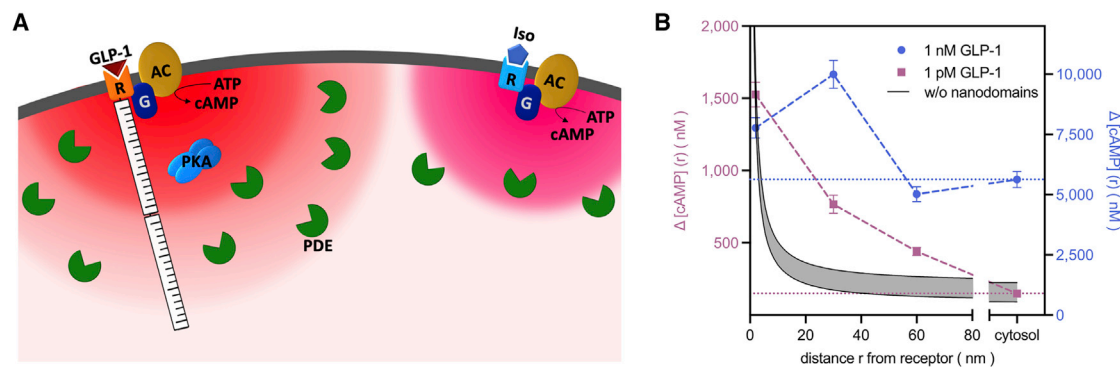


Figure 7. Model and quantitative considerations of RAINs

(A) At low agonist concentrations (i.e., low receptor occupancy), GPCRs (e.g., the GLP-1R, left) produce local cAMP pools (red gradient) that decrease at nanometer distances away from the GPCRs. Importantly, these RAINs appear not to overlap with RAINs of other receptors (e.g., β_2 -ARs, magenta gradient, right) and are shaped by localized PDE activity (green symbols). Within such RAINs, high local concentrations of cAMP cause strong activation of tethered PKA. At high agonist concentrations (i.e., higher receptor occupancy), RAINs increase in size and begin to merge, resulting in dissipation of cAMP gradients and, ultimately, in a generalized cellular cAMP response.

(B) Quantitative considerations of RAINs: cAMP concentration gradients do not obey the laws of simple diffusion. GLP-1-induced FRET changes of the four biosensors (cf. Figure 3) were converted into nanomolar cAMP increases (Δ [cAMP]) and plotted for 1 pM (magenta squares, left y axis) and 1 nM GLP-1 (blue circles, right y axis). Dashed lines connecting the data points are meant as a guide to show the geometry of RAINs at both GLP-1 concentrations. Horizontal dotted lines represent cytosolic cAMP after stimulation with 1 pM (magenta) and 1 nM GLP-1 (blue). The gray area displays the mean \pm 95% CI of a fit ($A(\text{nM} \times \text{nm}) = 1,376 [1,306; 1,446]$) assuming a $1/r$ dependency of the cAMP concentration (see main text, STAR Methods, and Methods S1).

stimulation and suggest that RAINs may be a general phenomenon of GPCRs.

Our data suggest that cells may use these RAINs to spatially limit distinct cAMP signals stemming from different GPCRs. This is based on three main findings. First, cAMP concentrations inside RAINs do not equilibrate with cytosolic cAMP over minutes. Second, cAMP pools generated by β_2 -ARs do not equilibrate with the cAMP pool inside the GLP-1R nanodomains; i.e., RAINs are protected from (low levels of) stimulation of other GPCRs. Third, disruption of PKA tethering inside RAINs abolishes the signaling function of this individual unit. We propose that by organizing extracellular GPCR stimuli into RAINs, cells are able to precisely sense which cAMP pool stems from which GPCR. Cells would thereby be capable of orchestrating distinct cAMP pools simultaneously and, ultimately, of relaying them into receptor-specific cell function with high spatial precision.

These findings have important implications for our understanding of GPCR signaling via cAMP. Traditionally, cAMP has been regarded as a freely diffusible messenger and, thus, would increase (or decrease) uniformly within an entire cell upon stimulation of adenylyl cyclase-linked GPCRs. This would mean that cAMP would allow cells to operate only as a single switch, being turned on or off via uniform cellular cAMP levels. However, we have shown recently that under physiological conditions cellular cAMP is largely bound and not freely diffusible (Bock et al., 2020), which would allow the formation of cAMP gradients. In line with this, we show here the existence of very small, independent cAMP signaling nanodomains around each individual GPCR. This indicates a huge number of cellular switches—with essentially each single GPCR representing one such unit—enlarging the complexity of cAMP signaling by orders of magnitude. Using an analogy from electronics, this would suggest that cAMP signaling of a cell does not represent a single transistor-

like switch but rather a chip comprising a large number of independent but interacting switches.

The possible number of such individual cAMP “switches” at the cell surface can be roughly estimated if we consider that the RAIN’s radius appears to be on the order of 60 nm; that is, their diameter about 120 nm. In order to assure a “safe” distance between individual switches, they may be placed at distances of ≈ 200 nm, i.e., at a density of $\approx 25/\mu\text{m}^2$. Considering that most cells have a surface area of several hundred μm^2 , this would allow for several thousand independent cAMP “switches.”

The molecular details of how such RAINs are shaped remain to be elucidated. Our data suggest at least two possible mechanisms. The first one is a marked reduction of the cAMP diffusion coefficient over a range of a few tens of nanometers from the receptor, which might be brought about by buffered diffusion combined with molecular crowding or formation of biomolecular condensates (Bock et al., 2020; Zhang et al., 2020). The second mechanism is substantially higher PDE concentrations close to receptors compared with the bulk cytosol, a mechanism that would be in line with our data showing that PDE inhibition is highly dependent on the distance from the receptor, suggesting differentially localized PDE activity (Figure 4).

The exact composition of RAINs, i.e., which proteins contribute to them, how they are organized, and whether they are stable or dynamic, also remains to be studied. While our data indicate that AKAPs, PKA, and PDEs are necessary constituents, other proteins may well contribute to the individual properties of individual RAINs.

Our model (Figure 7A) further suggests that upon stronger stimulation, the concentrations of cAMP begin to overcome the local PDE capacity, as well as the buffering capacity, for cAMP. This would increase the concentrations of free, diffusible cAMP and thereby cause dissipation and progressive fusion of

the individual RAINs, ultimately resulting in generalized increases of cAMP throughout a cell, which allows generalized activation of cAMP targets, including changes in gene transcription via cAMP response elements—processes that would appear to be unrelated to complex signaling via individual RAINs.

The level of receptor stimulation required to overcome RAINs should depend on a number of parameters. For example, a comparison of cytosolic cAMP signals induced by low levels of endogenous β_2 -ARs in HEK cells and those seen upon overexpression of β_2 -ARs illustrates that receptor levels have a strong impact (compare, e.g., [Figures 2E and 6D](#)). Likewise, the agonist concentration affects not only the amplitude but also the kinetics of cAMP signals in the different compartments (compare, e.g., [Figure 3B and 3C](#)). Levels of other protein components inside RAINs, such as PDEs and AKAPs, will also very significantly contribute to their size, shape, and function.

Taken together, our study reveals mechanisms of how cells can independently process large numbers of receptor signals by spatially restricting cAMP in nanometer-size RAINs. Localized cAMP signaling has been suggested by a number of studies to be important for normal cell homeostasis and function. As a consequence, a disruption of localized cAMP signaling has been proposed to be associated with various diseases ([Bers et al., 2019](#); [Gold et al., 2013](#); [Nikolaev et al., 2010](#); [Zaccolo et al., 2021](#); [Zhang et al., 2020](#)). Our data reveal the molecular mechanisms of how such localized cAMP signaling by individual GPCRs is brought about. They further suggest that modulation of individual RAIN signaling may hold therapeutic potential.

Limitations of the study

Our study demonstrates the existence of RAINs for two GPCRs—the class B GLP-1R and the class A β_2 -AR. It will be important to study, whether similar principles apply to other GPCRs, notably not only to G_s -coupled receptors that increase cAMP but also those triggering other signaling pathways. In addition, the cells being investigated are relatively simple cell culture lines, and it will be most interesting to see how cells with a more complex architecture, such as neurons or cardiomyocytes, may organize such signaling nanodomains. For example, it may be expected that individual RAINs will fuse at postsynaptic sites and that they may be unevenly distributed in cells where receptor distribution is not uniform, such as cardiomyocytes ([Bathe-Peters et al., 2021](#)). It will be important to see how stable RAINs may be, i.e., if they change over time, both short and long term, and how the mobility of receptors and signaling proteins ([Möller et al., 2020](#); [Sungkaworn et al., 2017](#)) may affect the shape and function of RAINs. And finally, it will be important to determine more accurately the stimulus strengths that lead to the formation and dissipation of the cAMP gradients that form RAINs.

STAR★METHODS

Detailed methods are provided in the online version of this paper and include the following:

- [KEY RESOURCES TABLE](#)

● RESOURCE AVAILABILITY

- Lead contact
- Materials availability
- Data and code availability

● EXPERIMENTAL MODEL AND SUBJECT DETAILS

● METHOD DETAILS

- Biosensor construction
- Single-cell Foerster Resonance Energy Transfer (FRET) imaging
- Confocal microscopy
- Direct Stochastic optical reconstruction microscopy (dSTORM)
- Sensor calibration
- cAMP ELISA
- cAMP accumulation assays by HTRF
- Forskolin-induced PKA phosphorylation
- Quantitative analysis of cAMP gradients at the nanometer scale

● QUANTIFICATION AND STATISTICAL ANALYSIS

SUPPLEMENTAL INFORMATION

Supplemental information can be found online at <https://doi.org/10.1016/j.cell.2022.02.011>.

ACKNOWLEDGMENTS

We thank Bärbel Pohl, Marlies Grieben, and Pauline Löffler for technical support and all members of the Lohse lab for valuable discussions on the manuscript. A.B., P.A., and M.J.L. acknowledge funding by the Deutsche Forschungsgemeinschaft (DFG) (German Research Foundation) through SFB1423, project number 421152132, subproject C03 (P.A. and M.J.L.) and subproject C05 (A.B.), and through SFB688, subproject B08 (M.J.L.). This work was supported by the Elite Network of Bavaria, Receptor Dynamics program (to M.J.L.). S.E.A. and J.M. were members of this program. I.M. is an Anne McLaren Research Fellow. This work was supported by the British Heart Foundation PG/15/5/31110 and RG/17/6/32944 (to M.Z.).

AUTHOR CONTRIBUTIONS

I.M., M.J.L., and A.B. conceived of the study. S.E.A., I.M., M.J.L., and A.B. designed experiments. S.E.A. and C.K. conducted the majority of experiments. S.E.A., C.K., I.M., K.N., and A.B. analyzed data. K.N. designed, conducted, and analyzed the functional characterization of biosensors. S.E.A. designed, conducted, and analyzed dSTORM experiments with the help of J.M. A.K. and M.Z. helped with sensor calibration experiments. P.A. and M.F. contributed to the conceptualization of the biophysical framework of RAINs. M.F. developed the mathematical details of RAINs. S.E.A., C.K., K.N., and A.B. prepared figures. A.B. and M.J.L. wrote the paper with contributions from S.E.A., C.K., I.M., K.N., and M.F. All authors edited the manuscript. M.J.L. initiated the project. A.B. and M.J.L. directed overall research.

DECLARATION OF INTERESTS

The authors have no conflicts of interest to declare.

Received: May 3, 2021
Revised: December 20, 2021
Accepted: February 9, 2022
Published: March 15, 2022

REFERENCES

- Agarwal, S.R., Clancy, C.E., and Harvey, R.D. (2016). Mechanisms restricting diffusion of intracellular cAMP. *Sci. Rep.* **6**, 19577.
- Agarwal, S.R., Yang, P.C., Rice, M., Singer, C.A., Nikolaev, V.O., Lohse, M.J., Clancy, C.E., and Harvey, R.D. (2014). Role of membrane microdomains in compartmentation of cAMP signaling. *PLoS One* **9**, e95835.
- Avet, C., Mancini, A., Breton, B., Le Gouill, C., Hauser, A.S., Normand, C., Kobayashi, H., Gross, F., Hogue, M., Lukasheva, V., et al. (2020). Selectivity landscape of 100 therapeutically relevant GPCR profiled by an effector translocation-based BRET platform. *SSRN Journal*, 2020.2004.2020.052027.
- Bacskaï, B.J., Hochner, B., Mahaut-Smith, M., Adams, S.R., Kaang, B.K., Kandel, E.R., and Tsien, R.Y. (1993). Spatially resolved dynamics of cAMP and protein kinase A subunits in *Aplysia* sensory neurons. *Science* **260**, 222–226.
- Baillie, G.S. (2009). Compartmentalized signalling: Spatial regulation of cAMP by the action of compartmentalized phosphodiesterases. *FEBS Journal* **276**, 1790–1799.
- Baillie, G.S., Tejada, G.S., and Kelly, M.P. (2019). Therapeutic targeting of 3',5'-cyclic nucleotide phosphodiesterases: Inhibition and beyond. *Nat. Rev. Drug Discov.* **18**, 770–796.
- Bathe-Peters, M., Gmach, P., Boltz, H.H., Einsiedel, J., Gotthardt, M., Hübner, H., Gmeiner, P., Lohse, M.J., and Annibale, P. (2021). Visualization of beta-adrenergic receptor dynamics and differential localization in cardiomyocytes. *Proc. Natl. Acad. Sci. USA* **118**, e2101119118.
- Bender, A.T., and Beavo, J.A. (2006). Cyclic nucleotide phosphodiesterases: molecular regulation to clinical use. *Pharmacol. Rev.* **58**, 488–520.
- Bentele, K., and Falcke, M. (2007). Quasi-steady approximation for ion channel currents. *Biophys. J.* **93**, 2597–2608.
- Bers, D.M., Xiang, Y.K., and Zaccolo, M. (2019). Whole-cell cAMP and PKA activity are epiphenomena, nanodomain signaling matters. *Physiology (Bethesda)* **34**, 240–249.
- Bock, A., Annibale, P., Konrad, C., Hannawacker, A., Anton, S.E., Maiellaro, I., Zabel, U., Sivaramakrishnan, S., Falcke, M., and Lohse, M.J. (2020). Optical mapping of cAMP signaling at the nanometer scale. *Cell* **182**, 1519–1530.e17.
- Börner, S., Schwede, F., Schlipp, A., Berisha, F., Calebiro, D., Lohse, M.J., and Nikolaev, V.O. (2011). FRET measurements of intracellular cAMP concentrations and cAMP analog permeability in intact cells. *Nat. Protoc.* **6**, 427–438.
- Brunton, L.L., Hayes, J.S., and Mayer, S.E. (1979). Hormonally specific phosphorylation of cardiac troponin I and activation of glycogen phosphorylase. *Nature* **280**, 78–80.
- Buxton, I.L., and Brunton, L.L. (1983). Compartments of cyclic AMP and protein kinase in mammalian cardiomyocytes. *J. Biol. Chem.* **258**, 10233–10239.
- Chen, C., Nakamura, T., and Koutalos, Y. (1999). Cyclic AMP diffusion coefficient in frog olfactory cilia. *Biophys. J.* **76**, 2861–2867.
- Civciristov, S., Ellisdon, A.M., Suderman, R., Pon, C.K., Evans, B.A., Kleinfeld, O., Charlton, S.J., Hlavacek, W.S., Canals, M., and Halls, M.L. (2018). Pre-assembled GPCR signaling complexes mediate distinct cellular responses to ultralow ligand concentrations. *Sci. Signal.* **11**, eaan1188.
- Depry, C., Allen, M.D., and Zhang, J. (2011). Visualization of PKA activity in plasma membrane microdomains. *Mol. Biosyst.* **7**, 52–58.
- Di Benedetto, G., Zoccarato, A., Lissandron, V., Terrin, A., Li, X., Houslay, M.D., Baillie, G.S., and Zaccolo, M. (2008). Protein kinase A type I and type II define distinct intracellular signaling compartments. *Circ. Res.* **103**, 836–844.
- Drucker, D.J. (2018). Mechanisms of action and therapeutic application of glucagon-like Peptide-1. *Cell Metab.* **27**, 740–756.
- Drucker, D.J., Habener, J.F., and Holst, J.J. (2017). Discovery, characterization, and clinical development of the glucagon-like peptides. *J. Clin. Invest.* **127**, 4217–4227.
- Fischmeister, R., Castro, L.R., Abi-Gerges, A., Rochais, F., Jurevicius, J., Leroy, J., and Vandecasteele, G. (2006). Compartmentation of cyclic nucleotide signaling in the heart: the role of cyclic nucleotide phosphodiesterases. *Circ. Res.* **99**, 816–828.
- Fletcher, M.M., Halls, M.L., Christopoulos, A., Sexton, P.M., and Wootten, D. (2016). The complexity of signalling mediated by the glucagon-like peptide-1 receptor. *Biochem. Soc. Trans.* **44**, 582–588.
- Fredriksson, R., Lagerström, M.C., Lundin, L.G., and Schiöth, H.B. (2003). The G-protein-coupled receptors in the human genome form five main families. Phylogenetic analysis, paralogon groups, and fingerprints. *Mol. Pharmacol.* **63**, 1256–1272.
- Gibson, D.G., Young, L., Chuang, R.Y., Venter, J.C., Hutchison, C.A., 3rd, and Smith, H.O. (2009). Enzymatic assembly of DNA molecules up to several hundred kilobases. *Nat. Methods* **6**, 343–345.
- Gold, M.G., Gonen, T., and Scott, J.D. (2013). Local cAMP signaling in disease at a glance. *J. Cell Sci.* **126**, 4537–4543.
- Halls, M.L., and Cooper, D.M. (2010). Sub-picomolar relaxin signalling by a pre-assembled RXFP1, AKAP79, AC2, beta-arrestin 2, PDE4D3 complex. *EMBO J.* **29**, 2772–2787.
- Hauser, A.S., Attwood, M.M., Rask-Andersen, M., Schiöth, H.B., and Gloriam, D.E. (2017). Trends in GPCR drug discovery: new agents, targets and indications. *Nat. Rev. Drug Discov.* **16**, 829–842.
- Hayes, J.S., Brunton, L.L., Brown, J.H., Reese, J.B., and Mayer, S.E. (1979). Hormonally specific expression of cardiac protein kinase activity. *Proc. Natl. Acad. Sci. USA* **76**, 1570–1574.
- Hayes, J.S., Brunton, L.L., and Mayer, S.E. (1980). Selective activation of particulate cAMP-dependent protein kinase by isoproterenol and prostaglandin E1. *J. Biol. Chem.* **255**, 5113–5119.
- Houslay, M.D. (2010). Underpinning compartmentalised cAMP signalling through targeted cAMP breakdown. *Trends Biochem. Sci.* **35**, 91–100.
- Huang, R.C., and Gillette, R. (1993). Co-regulation of cAMP-activated Na⁺ current by Ca²⁺ in neurones of the mollusc Pleurobranchaea. *J. Physiol.* **462**, 307–320.
- Inoue, A., Raimondi, F., Kadji, F.M.N., Singh, G., Kishi, T., Uwamizuru, A., Ono, Y., Shinjo, Y., Ishida, S., Arang, N., et al. (2019). Illuminating G-protein-coupling selectivity of GPCRs. *Cell* **177**, 1933–1947.e25.
- Insel, P.A., Wilderman, A., Zamboni, A.C., Snead, A.N., Murray, F., Aroonsakool, N., McDonald, D.S., Zhou, S., McCann, T., Zhang, L., et al. (2015). G protein-coupled receptor (GPCR) expression in native cells: “novel” endoGPCRs as physiologic regulators and therapeutic targets. *Mol. Pharmacol.* **88**, 181–187.
- Koschinski, A., and Zaccolo, M. (2015). A novel approach combining real-time imaging and the patch-clamp technique to calibrate FRET-based reporters for cAMP in their cellular microenvironment. *Methods Mol. Biol.* **1294**, 25–40.
- Langeberg, L.K., and Scott, J.D. (2015). Signalling scaffolds and local organization of cellular behaviour. *Nat. Rev. Mol. Cell Biol.* **16**, 232–244.
- Lefkimmatis, K., and Zaccolo, M. (2014). cAMP signaling in subcellular compartments. *Pharmacol. Ther.* **143**, 295–304.
- Lester, L.B., Langeberg, L.K., and Scott, J.D. (1997). Anchoring of protein kinase A facilitates hormone-mediated insulin secretion. *Proc. Natl. Acad. Sci. USA* **94**, 14942–14947.
- Lohse, C., Bock, A., Maiellaro, I., Hannawacker, A., Schad, L.R., Lohse, M.J., and Bauer, W.R. (2017). Experimental and mathematical analysis of cAMP nanodomains. *PLoS One* **12**, e0174856.
- Maiellaro, I., Lohse, M.J., Kittel, R.J., and Calebiro, D. (2016). cAMP signals in *Drosophila* motor neurons are confined to single synaptic boutons. *Cell Rep.* **17**, 1238–1246.
- Martiel, J.L., and Goldbeter, A. (1987). A model based on receptor desensitization for cyclic AMP signaling in *Dictyostelium* cells. *Biophys. J.* **52**, 807–828.
- Möller, J., Isbilir, A., Sungkaworn, T., Osberg, B., Karathanasis, C., Sunkara, V., Grushevskiy, E.O., Bock, A., Annibale, P., Heilemann, M., et al. (2020). Single-molecule analysis reveals agonist-specific dimer formation of micro-opioid receptors. *Nat. Chem. Biol.* **16**, 946–954.
- Müller, T.D., Finan, B., Bloom, S.R., D'Alessio, D., Drucker, D.J., Flatt, P.R., Fritsche, A., Gribble, F., Grill, H.J., Habener, J.F., et al. (2019). Glucagon-like peptide 1 (GLP-1). *Mol. Metab.* **30**, 72–130.

- Nikolaev, V.O., Bünemann, M., Hein, L., Hannawacker, A., and Lohse, M.J. (2004). Novel single chain cAMP sensors for receptor-induced signal propagation. *J. Biol. Chem.* *279*, 37215–37218.
- Nikolaev, V.O., Bünemann, M., Schmitteckert, E., Lohse, M.J., and Engelhardt, S. (2006). Cyclic AMP imaging in adult cardiac myocytes reveals far-reaching beta1-adrenergic but locally confined beta2-adrenergic receptor-mediated signaling. *Circ. Res.* *99*, 1084–1091.
- Nikolaev, V.O., Moshkov, A., Lyon, A.R., Miragoli, M., Novak, P., Paur, H., Lohse, M.J., Korchev, Y.E., Harding, S.E., and Gorelik, J. (2010). Beta2-adrenergic receptor redistribution in heart failure changes cAMP compartmentation. *Science* *327*, 1653–1657.
- Ovesný, M., Křížek, P., Borkovec, J., Svindrych, Z., and Hagen, G.M. (2014). ThunderSTORM: a comprehensive ImageJ plug-in for PALM and STORM data analysis and super-resolution imaging. *Bioinformatics* *30*, 2389–2390.
- Pándy-Szekeres, G., Munk, C., Tsonkov, T.M., Mordalski, S., Harpsøe, K., Hauser, A.S., Bojarski, A.J., and Gloriam, D.E. (2018). GPCRdb in 2018: adding GPCR structure models and ligands. *Nucleic Acids Res.* *46*, D440–D446.
- Rich, T.C., Fagan, K.A., Nakata, H., Schaack, J., Cooper, D.M., and Karpen, J.W. (2000). Cyclic nucleotide-gated channels colocalize with adenylyl cyclase in regions of restricted cAMP diffusion. *J. Gen. Physiol.* *116*, 147–161.
- Rich, T.C., Fagan, K.A., Tse, T.E., Schaack, J., Cooper, D.M., and Karpen, J.W. (2001). A uniform extracellular stimulus triggers distinct cAMP signals in different compartments of a simple cell. *Proc. Natl. Acad. Sci. U. S. A.* *98*, 13049–13054.
- Rich, T.C., Xin, W., Mehats, C., Hassell, K.A., Piggott, L.A., Le, X., Karpen, J.W., and Conti, M. (2007). Cellular mechanisms underlying prostaglandin-induced transient cAMP signals near the plasma membrane of HEK-293 cells. *Am. J. Physiol. Cell Physiol.* *292*, C319–C331.
- Richards, M., Lomas, O., Jalink, K., Ford, K.L., Vaughan-Jones, R.D., Lefkimiatis, K., and Swietach, P. (2016). Intracellular tortuosity underlies slow cAMP diffusion in adult ventricular myocytes. *Cardiovasc. Res.* *110*, 395–407.
- Rosenbaum, D.M., Rasmussen, S.G., and Kobilka, B.K. (2009). The structure and function of G-protein-coupled receptors. *Nature* *459*, 356–363.
- Schihada, H., Nemeč, K., Lohse, M.J., and Maiellaro, I. (2021). Bioluminescence in G protein-coupled receptors drug screening using nanoluciferase and halo-tag technology. *Methods Mol. Biol.* *2268*, 137–147.
- Schneider, C.A., Rasband, W.S., and Eliceiri, K.W. (2012). NIH Image to ImageJ: 25 years of image analysis. *Nat. Methods* *9*, 671–675.
- Scott, J.D., and Pawson, T. (2009). Cell signaling in space and time: where proteins come together and when they're apart. *Science* *326*, 1220–1224.
- Sivaramakrishnan, S., and Spudich, J.A. (2011). Systematic control of protein interaction using a modular ER/K alpha-helix linker. *Proc. Natl. Acad. Sci. USA* *108*, 20467–20472.
- Southan, C., Sharman, J.L., Benson, H.E., Faccenda, E., Pawson, A.J., Alexander, S.P., Buneman, O.P., Davenport, A.P., McGrath, J.C., Peters, J.A., et al. (2016). The IUPHAR/BPS Guide to PHARMACOLOGY in 2016: Towards curated quantitative interactions between 1300 protein targets and 6000 ligands. *Nucleic Acids Res.* *44*, D1054–D1068.
- Sriram, K., and Insel, P.A. (2018). G protein-coupled receptors as targets for approved drugs: How many targets and how many drugs? *Mol. Pharmacol.* *93*, 251–258.
- Stangherlin, A., and Zaccolo, M. (2012). Phosphodiesterases and subcellular compartmentalized cAMP signaling in the cardiovascular system. *Am. J. Physiol. Heart Circ. Physiol.* *302*, H379–H390.
- Sungkaworn, T., Jobin, M.L., Burnecki, K., Weron, A., Lohse, M.J., and Calebiro, D. (2017). Single-molecule imaging reveals receptor-G protein interactions at cell surface hot spots. *Nature* *550*, 543–547.
- Surdo, N.C., Berrera, M., Koschinski, A., Brescia, M., Machado, M.R., Carr, C., Wright, P., Gorelik, J., Morotti, S., Grandi, E., et al. (2017). FRET biosensor uncovers cAMP nano-domains at beta-adrenergic targets that dictate precise tuning of cardiac contractility. *Nat. Commun.* *8*, 15031.
- Taylor, S.S., Ilouz, R., Zhang, P., and Kornev, A.P. (2012). Assembly of allosteric macromolecular switches: Lessons from PKA. *Nat. Rev. Mol. Cell Biol.* *13*, 646–658.
- Tovey, S.C., Dedos, S.G., Taylor, E.J., Church, J.E., and Taylor, C.W. (2008). Selective coupling of type 6 adenylyl cyclase with type 2 IP3 receptors mediates direct sensitization of IP3 receptors by cAMP. *J. Cell Biol.* *183*, 297–311.
- Violin, J.D., DiPilato, L.M., Yildirim, N., Elston, T.C., Zhang, J., and Lefkowitz, R.J. (2008). Beta2-adrenergic receptor signaling and desensitization elucidated by quantitative modeling of real time cAMP dynamics. *J. Biol. Chem.* *283*, 2949–2961.
- Weis, W.I., and Kobilka, B.K. (2018). The molecular basis of G protein-coupled receptor activation. *Annu. Rev. Biochem.* *87*, 897–919.
- Wong, W., and Scott, J.D. (2004). AKAP signalling complexes: Focal points in space and time. *Nat. Rev. Mol. Cell Biol.* *5*, 959–970.
- Zaccolo, M., Zerio, A., and Lobo, M.J. (2021). Subcellular organization of the cAMP signaling pathway. *Pharmacol. Rev.* *73*, 278–309.
- Zhang, J.Z., Lu, T.W., Stolerman, L.M., Tenner, B., Yang, J.R., Zhang, J.F., Falcke, M., Rangamani, P., Taylor, S.S., Mehta, S., et al. (2020). Phase separation of a PKA regulatory subunit controls cAMP compartmentation and oncogenic signaling. *Cell* *182*, 1531–1544.e15.
- Zhao, P., Liang, Y.L., Belousoff, M.J., Deganutti, G., Fletcher, M.M., Willard, F.S., Bell, M.G., Christie, M.E., Sloop, K.W., Inoue, A., et al. (2020). Activation of the GLP-1 receptor by a non-peptidic agonist. *Nature* *577*, 432–436.

STAR★METHODS

KEY RESOURCES TABLE

REAGENT or RESOURCE	SOURCE	IDENTIFIER
Bacterial and Virus Strains		
NEB 5-alpha Competent E.coli (High Efficiency)	New England Biolabs	Cat#: C2987
XL1-Blue Competent Cells	Agilent	Cat#: 200249
Chemicals, Peptides, and Recombinant Proteins		
(-)-Isoproterenol hydrochloride	Sigma-Aldrich	Cat#: I6504; CAS: 5984-95-2
3-isobutyl-1-methylxanthin (IBMX)	Sigma-Aldrich	Cat#: I5879; CAS: 28822-58-4
8-Br-2'-O-Me-cAMP-AM	BIOLOG Life Science Institute	Cat#: B028
Adenosine 3',5'-cyclic monophosphate sodium salt monohydrate (cAMP)	Sigma-Aldrich	Cat#: A6885; CAS: 37839-81-9
Effectene Transfection Reagent	Qiagen	Cat#: 301427
Forskolin	BioTrend	Cat#: AOB6380-5; CAS: 66575-29-9
FuGENE HD transfection reagent	Promega	Cat#: E2311
Gibson Assembly Master Mix	New England Biolabs, (Gibson et al., 2009)	Cat#: E2611
GLP-1-(7-36)-amide	Tocris	Cat#: 2082; CAS: 107444-51-9
InCELLect AKAP St-Ht31 Inhibitor Peptide (St-Ht31)	Promega	Cat#: V8211
InCELLect AKAP St-Ht31 Control Peptide (St-Ht31-P)	Promega	Cat#: V8221
JF-646 Halo dye	Dr. Luke Lavis (Janelia Research Campus, Virginia, USA)	N/A
Lipofectamine 2000	Invitrogen	Cat#: 11668030
Lipofectamine 3000	Invitrogen	Cat#: L3000008
MDL-12,330A hydrochloride	Sigma-Aldrich	Cat#: M182, CAS: 40297-09-4
Saponin from Quillaja sp.	Sigma-Aldrich	Cat#: S4521, CAS: 8047-15-2
Critical Commercial Assays		
Cyclic AMP ELISA Kit	Cayman Chemicals	Cat#: 581001
cAMP Gs Dynamic kit HTRF	Cisbio	Cat#: 62AM4PEB
cAMP Gs HiRange kit HTRF	Cisbio	Cat#: 62AM6PEB
Experimental Models: Cell Lines		
CHO-K1 CCL-61	ATCC	Cat#: CCL61
HEK-tsA201 cells	Sigma-Aldrich	ECACC Cat# 96121229
HEK-293AD cells	BioCat	Cat# AD-100-GVO-CB
Oligonucleotides		
Primers for Cloning, see Table S2	This paper	Table S2
Recombinant DNA		
β_2 AR-camps	This paper	N/A
β_2 AR-IRES2-Epac1-camps	This paper	N/A
β_2 AR-IRES2-Epac1-camps-CAAX	This paper	N/A
Epac1-camps	(Nikolaev et al., 2004)	N/A
Epac1-camps-CAAX	This paper	N/A
GLP-1R	Dr. Christoph Klenk (University of Zürich, Switzerland)	N/A
GLP1R-AKAR4	This paper	N/A
GLP1R-camps	This paper	N/A
GLP1R-camps-R279E	This paper	N/A
GLP1R-IRES2-AKAR4	This paper	N/A

(Continued on next page)

Continued

REAGENT or RESOURCE	SOURCE	IDENTIFIER
GLP1R-IRES2-Epac1-camps	This paper	N/A
GLP1R-IRES2-Epac1-camps-CAAX	This paper	N/A
GLP1R-SAH30-camps	This paper	N/A
GLP1R-SAH60-camps	This paper	N/A
pcDNA3-AKAR4	Dr. Jin Zhang (UC San Diego, USA) (Depry et al., 2011)	Addgene Plasmid #61619
SAH60 linker	synthesized by Eurofins genomics, Ebersberg, Germany	N/A
SPASM sensor with 30 nm ER/K α -helix	Sivaramakrishnan and Spudich (2011)	N/A
Software and Algorithms		
GraphPad Prism software 7.0, 8.1.2, 9.1	GraphPad Software	https://www.graphpad.com/scientific-software/prism/
ImageJ, Thunderstorm plugin	(Schneider et al, 2012) (Ovesny et al., 2014)	N/A
OriginPro	OriginLab Corporation	https://www.originlab.com/origin
VisiView 4.0 imaging software	Visitron Systems	https://www.visitron.de/products/visiviewr-software.html

RESOURCE AVAILABILITY

Lead contact

Further information and request for resources and reagents should be directed to and will be fulfilled by the lead contact Martin J. Lohse (martin.lohse@isarbioscience.de).

Materials availability

All plasmids generated in this study are available from the authors upon request and require a Materials Transfer Agreement.

Data and code availability

- All data reported in this paper will be shared by the lead contact upon request.
- This paper does not report original code.
- Any additional information required to reanalyze the data reported in this paper is available from the lead contact upon request.

EXPERIMENTAL MODEL AND SUBJECT DETAILS

HEK-tsA201 (ECACC 96121229, Sigma-Aldrich Chemie GmbH, referred to as HEK cells throughout the manuscript), HEK-293AD (AD-100-GVO-CB, BioCat GmbH, Heidelberg, Germany, referred to as HEK-AD cells throughout the manuscript) and CHO-K1 cells (CCL-61™, ATCC, Teddington, UK, referred to as CHO cells throughout the manuscript) were cultured in complete DMEM with 4.5 g/L glucose (PAN Biotech, Aidenbach, Germany), or DMEM/Ham's F12 (Life Technologies GmbH, Darmstadt, Germany) respectively, both supplemented with 10 % (v/v) fetal bovine serum (Biochrom GmbH, Berlin, Germany), 100 U/mL penicillin, 100 μ g/mL streptomycin (Pen/Strep, GIBCO Life technologies, Carlsbad, CA, USA) and 2 mM L-glutamine (PAN Biotech, Aidenbach, Germany) at 37 °C and 5 % CO₂. Cells were passaged in T75 flasks every 2-4 days when reaching a confluency of 80-90 %. Cells were routinely tested for mycoplasma contamination using MycoAlert™ Mycoplasma Detection Kit from Lonza (Basel, Switzerland). Cell lines were not contaminated with mycoplasma.

For fluorescence microscopy experiments, HEK cells and HEK-AD cells (used for β_2 -AR biosensors) were seeded on Poly-D-Lysine-coated 24 mm glass cover slips in 6-well plates and transfected with 300-600 ng cDNA per cover slip using Effectene transfection reagent (Qiagen, Hilden, Germany) as follows: for transfection of one well of a 6-well plate, 300-600 ng cDNA was mixed with 66 μ L buffer EC and 3.2 μ L Enhancer and was incubated for 2 min. 7 μ L Effectene transfection reagent was added and the mixture was incubated for 20 min at room temperature. After addition of 350 μ L prewarmed cell culture medium, 400 μ L of the mixture was added dropwise to the cells. Culture medium was renewed 24 h after transfection. Fluorescence microscopy experiments were performed 24-48 h (GLP1R-camps, GLP1R-IRES2-Epac1-camps, GLP1R-IRES2-Epac1-camps-CAAX, GLP1R-AKAR4, GLP1R-IRES2-AKAR4, β_2 AR-camps, β_2 AR-IRES2-Epac1-camps, β_2 AR-IRES2-Epac1-camps-CAAX, Epac1-camps, and Epac1-camps-CAAX) or 64-72 h (GLP1R-SAH30-camps and GLP1R-SAH60-camps) after transfection.

For sensor calibration experiments, CHO cells were seeded on uncoated cover slips into 6-well plates and transfected with 2 μ g cDNA per cover slip using FuGENE HD transfection reagent (Promega) at a 3:1 ratio. cDNA was mixed with Opti-MEM and FuGENE HD transfection reagent was added. The mixture was incubated for 12 min at room temperature before it was added to the cells. 24 h after transfection culture medium was renewed and fluorescence microscopy experiments were conducted 48 h post transfection.

For dSTORM imaging, CHO cells were seeded the night before on uncoated cover slips into 6-well plates. 12–14 h after seeding, cells were transfected with 2 μ g cDNA per cover slip using LipofectamineTM 2000. The conditions for one well of a 6-well plate are as follows: 2 μ g of cDNA and 6 μ L LipofectamineTM 2000 transfection reagent were each mixed separately with 500 μ L Opti-MEM, incubated for 5 min at room temperature before being combined. The transfection mixture was incubated for 20 min at room temperature. During incubation the cells were washed twice with PBS and kept in phenol red-free DMEM/F12 medium with 10 % FCS with no antibiotics. The transfection mixture was added to each well. 4–5 h after transfection cells were labelled and fixed. dSTORM experiments were conducted on the same day or 24 h later.

For cAMP determinations by ELISA, HEK cells were seeded at a density of 2.5×10^5 cells/well into 6 well plates and left to adhere overnight. Cells were transfected with either wild-type GLP-1R or *GLP1R-camps* using a calcium phosphate transfection protocol (3 μ g cDNA, 3 μ g empty pcDNA3, 125 mM CaCl₂, 25 mM N,N-bis[2-hydroxyethyl]-2-aminoethanesulfonic acid, 140 mM NaCl, 0.75 mM Na₂HPO₄ x 2 H₂O, pH=6.95 adjusted at 20°C) incubation for 20 min, adding to the cells). 24 h after transfection culture medium was renewed.

For HTRF experiments to determine cAMP accumulation by GLP-1R biosensors, HEK cells were seeded at a density of 1.3×10^6 cells into a 6 cm dish and left to adhere overnight. Cells were transfected after 24 h with 6 μ g of cDNA using LipofectamineTM 3000 (InvitrogenTM). Briefly, 6 μ g cDNA was mixed with 12 μ L P3000 reagent and 300 μ L Opti-MEM (i.e. mix 1). 18 μ L of LipofectamineTM 3000 was mixed with 300 μ L Opti-MEM (i.e. mix 2). Mix 1 and mix 2 were vortexed and combined to get the final solution and incubated at room temperature for 15 min. The final transfection mix was added dropwise to the cells. On the next day medium was renewed.

For HTRF experiments to determine cAMP accumulation by β_2 -AR biosensors, CHO cells were seeded at a density of 4×10^5 cells/well into a 6-well plate and left to adhere overnight. Cells were transfected after 24 h with 2 μ g of cDNA using LipofectamineTM 2000 (InvitrogenTM). Cells were washed twice with prewarmed PBS and prewarmed cell culture medium without antibiotics was added. Per well of a six-well plate 2 mixtures were prepared. In one tube 150 μ L Opti-MEM (reduced serum medium, no phenol red (GibcoTM)) was mixed with 2 μ g cDNA, in another tube 150 μ L Opti-MEM was mixed with 3.75 μ L LipofectamineTM 2000. Both mixtures were incubated at room temperature for 5 min and were combined afterwards. After another 10 min incubation 300 μ L of this mixture was added dropwise to the cells. 6 h after transfection medium was renewed.

For PKA phosphorylation assays using *AKAR4* biosensors, HEK cells were seeded at a density of 1.3×10^6 into a 6 cm dish and left to adhere overnight. Cells were transfected after 24 h with 1.5 μ g cDNA using Effectene transfection reagent. Briefly, 150 μ L buffer EC was mixed with 1.5 μ g cDNA. 12 μ L Enhancer was added and the mix was vortexed and incubated for 3 min. 24 μ L Effectene was added, mixed and incubated for 10 min at room temperature. The solution was added dropwise to the cells. On the next day medium was renewed.

METHOD DETAILS

Biosensor construction

All cAMP sensor constructs were cloned into pcDNA3. The cDNA for the wild-type human GLP-1R (a kind gift from Dr. Christoph Klenk, University of Zürich, Switzerland) was cloned in frame into a vector containing EYFP using HindIII and XbaI to generate GLP-1R-EYFP. To insert restriction sites for BmtI and BspEI between the GLP-1R and EYFP as well as restriction sites for EcoRI and NotI at the C terminus of EYFP, the following primers were used to amplify EYFP (#1: forward: 5'- AAA TCT AGA GCT AGC GGG TCC GGA GTG AGC AAG GGC GAG GAG - 3'; #2: reverse 5'- AAA AGC GGC CGC AAA GAA TTC CTT GTA CAG CTC GTC CAT - 3' priming sequence underlined, restriction sites in italics). In the following step *Epac1(E157-E316)*-CFP was cloned in frame into GLP-1R-EYFP using EcoRI and NotI thereby creating *GLP1R-Epac1-camps*. *GLP1R-camps-R279E* was generated by replacing *Epac1(E157-E316)*-CFP in *GLP1R-camps* with (*Epac1(E157-E317[R279E])*-CFP) using EcoRI and NotI. The 30 nm ER/K linker (a kind gift from Dr. Sivaraj Sivaramakrishnan, University of Minnesota, Minneapolis, USA) and 60 nm ER/K linker (synthesized by Eurofins genomics, Ebersberg, Germany) were inserted between GLP-1R and *Epac1-camps* using restriction enzymes BmtI and BspEI. *Epac1-camps-CAAX* was generated starting from *Epac2-camps-CAAX*. CFP-CAAX was cut out using XbaI and XhoI and inserted into *Epac1-camps* instead of the original CFP.

AKAR 4 was a kind gift from Dr. Jin Zhang, University of California San Diego, USA. *GLP1R-AKAR4* and *GLP1R-IRES2-AKAR4* were generated by Gibson cloning (Gibson et al., 2009). For *GLP1R-AKAR4* the insert GLP-1R was PCR amplified using a pair of primers (#3: forward: 5'- CCC AAG CTT GCG GCC GCC ACC ATG GCC GGC GCC CCC GGC - 3', #4: reverse: 5' - GCT CAC CAT GGG ATC CTT ATC TCC GGA CCC GCT AGC TCT AGA - 3'), and inserted upstream of *AKAR4* in its vector (#5: forward: 5' - TCT AGA GCT AGC GGG TCC GGA GAT AAG GAT CCC ATG GTG AGC - 3', #6: reverse: 5' - CGG GCC GGG GGC GCC GGC CAT GGT GGC GGC CGC AAG CTT - 3'). For *GLP1R-IRES2-AKAR4* an IRES2 sequence was PCR amplified as an insert using indicated primers (#7: forward: 5' - AGA GCT AGC GGG TCC GGA TAA GCC CCT CTC CCT CCC - 3', #8: reverse: 5' - CTC GCC CTT

GCT CAC CAT TGT GGC CAT ATT ATC ATC - 3'). IRES2 was then inserted between GLP-1R and AKAR4 in the construct *GLP1R-AKAR4* (#9: forward: 5' - GAT GAT AAT ATG GCC ACA ATG GTG AGC AAG GGC GAG - 3', #10: reverse: 5' - GGG AGG GAG AGG GGC TTA TCC GGA CCC GCT AGC TCT - 3').

For *GLP1R-IRES2-Epac1-camps* and *GLP1R-IRES2-Epac1-camps-CAAX*, the sequence encoding GLP1R-IRES2 from the template *GLP1R-IRES2-AKAR4* was PCR amplified using indicated primers (#11: forward: 5' - CTC ACT ATA GGG AGA CCC AAG CTT ATG GCC GGC GCC CCC GGC CCG CTG - 3', #12: reverse: 5' - CAG CTC CTC GCC CTT GCT CAC CAT TGT GGC CAT ATT ATC ATC GTG TTT - 3'). GLP1R-IRES2 was then inserted upstream of *Epac1-camps* or *Epac1-camps-CAAX* in its respective vector (#13: forward: 5' - AAA CAC GAT GAT AAT ATG GCC ACA ATG GTG AGC AAG GGC GAG GAG CTG - 3', #14: reverse: 5' - CAG CGG GCC GGG GGC GCC GGC CAT AAG CTT GGG TCT CCC TAT AGT GAG - 3'). To generate β_2AR -*camps*, in a first step, the upstream haemagglutinin signal peptide and downstream BmtI and BspEI restriction sites were inserted into a human β_2AR wild-type sequence by PCR amplification and Gibson cloning using indicated primers (#15: forward: 5' - ATA GGG AGA CCC AAG CTT ATG AAG ACC ATC ATC GCC CTG AGC - 3', #16: reverse: 5' - AAA TCC GGA CCC GCT AGC CAG CAG TGA GTC ATT TGT - 3'). In a second step, this β_2AR sequence was inserted into the *GLP1R-camps* template - where it replaced the GLP-1R wild-type sequence - using restriction enzyme cloning.

To clone β_2AR -*IRES2-Epac1-camps* and β_2AR -*IRES2-Epac1-camps-CAAX*, the β_2AR sequence was PCR amplified using indicated primers (#17: forward: 5' - CTC ACT ATA GGG AGA CCC AAG CTT ATG AAG ACC ATC ATC GCC CTG AGC - 3', #18: reverse: 5' - TAG GGG GGG GGG AGG GAG AGG GGC TTA TCC GGA CCC GCT AGC CAG CAG TGA - 3'). β_2AR was then inserted upstream of *IRES2-Epac1-camps* and *IRES2-Epac1-camps-CAAX* in its vectors *GLP1R-IRES2-Epac1-camps* and *GLP1R-IRES2-Epac1-camps-CAAX*, respectively, using the following pair of primers (#19: forward: 5' - TCA CTG CTG GCT AGC GGG TCC GGA TAA GCC CCT CTC CCT CCC CCC CTA - 3', #20: reverse: 5' - GCT CAG GGC GAT GAT GGT CTT CAT AAG CTT GGG TCT CCC TAT AGT GAG - 3'). Lyn-Halo-SAH60-Halo-CAAX was synthesized by Genescript, Piscataway, USA. All *AKAR4* constructs and Lyn-Halo-SAH60-Halo-CAAX were expressed in pcDNA3.1. Sequences were validated by sequencing of each construct by Eurofins or LGC genomics. All primer sequences are compiled in Table S2. All constructs derived by restriction enzyme cloning or Gibson cloning were transformed and amplified in XL1-Blue competent E.coli (Agilent) or NEB® 5-alpha Competent E.coli (New England Biolabs GmbH), respectively.

Single-cell Foerster Resonance Energy Transfer (FRET) imaging

For single-cell FRET imaging experiments, transfected cells were washed once and maintained in FRET buffer (10 mM HEPES, 140 mM NaCl, 5.4 mM KCl, 1 mM MgCl₂, 2 mM CaCl₂ (pH=7.4)) at room temperature throughout the experiment. Experiments were conducted on an Axiovert 200 inverted microscope (Zeiss, Jena, Germany) equipped with an oil immersion objective (plan-NEOFLUAR 63x/1.25), a 505 dcxr beam splitter (Visitron Systems, Puchheim, Germany), a xenon lamp coupled to a high speed polychromator system (Visitron Systems), an iXon Ultra EMCCD camera (Andor, Belfast, UK), and Metafluor 7 software (Molecular Devices, Sunnyvale, CA, USA); or on a Leica DMI8 inverted microscope (Leica Microsystems, Wetzlar, Germany) with an oil immersion objective (HC PL APO 63x/1,40-0,60 oil), a dichroic beamsplitter T505lpxr (Visitron Systems), a xenon lamp coupled to Visichrome high speed polychromator (Visitron Systems), a Photometrics Prime 95B sCMOS camera (Visitron systems) with Optosplit II dual emission image splitter (Cairn research, Faversham, UK), and Visiview 4.0 imaging software (Visitron Systems). Donor excitation occurred at 436 nm for 100 ms every 5 seconds and fluorescent images in the donor and acceptor emission channels (480 nm and 535 nm, respectively) were recorded every 5 seconds. Raw emission intensities were background-corrected by subtracting the fluorescence intensity of a cell-free region. Further, bleed-through of donor emission into the acceptor channel was subtracted as described previously (Börner et al., 2011): For all *Epac1-camps*-based sensors, corrected FRET ratios were calculated as the ratio between background-corrected donor emission (I_{donor}) at 480 nm and background and bleed-through-corrected acceptor emission ($I_{acceptor, corr}$) at 535 nm ($I_{donor} / I_{acceptor, corr}$). For *AKAR4*-based sensors the FRET ratio was calculated as the background and bleed-through-corrected acceptor emission over background corrected donor emission ($I_{acceptor, corr} / I_{donor}$). Drift corrected FRET traces were normalized ($\Delta FRET$ (% max)) to the basal ratio before compound addition (set to 0%) and maximum stimulus elicited by 10 μ M forskolin and 100 μ M IBMX at the end of each experiment (set to 100 %). Representative FRET traces in Figures 2, 5 and 6 were smoothed using adjacent average with 2nd order polynomial smoothing function.

Confocal microscopy

Cells were washed once and maintained in FRET buffer. Confocal images were obtained on a Leica TCS SP8 laser scanning microscope with an oil immersion objective (HC PL APO 63x/1,40 oil). A 514 nm laser was used at 5 % power to excite acceptor fluorophores and the respective emission was measured within 520-600 nm. Images were acquired with a hybrid detector in photon counting mode (1024 x 1024 pixel, line average 4, 400 Hz).

Direct Stochastic optical reconstruction microscopy (dSTORM)

After labeling cells transiently expressing the SAH60 construct with 1 μ M of the HaloTag® ligand JF-646 for 20 min at 37°C, they were fixed for 30 min with ice-cold methanol at -20°C. During imaging, samples were kept in Glox buffer (0.56 mg/mL glucose oxidase, 34 μ g/mL catalase, 10 % glucose, 0.1 M mercaptoethylamine, 50 mM Tris, 10 mM NaCl (pH=8.0)), at room temperature. dSTORM images were acquired on a TIRF illuminated Nikon Eclipse Ti2 microscope (Nikon, Tokyo, Japan) equipped with a 100 x objective with

a 1.49 NA automated correction collar; 405, 488, 561, 647 nm laser diodes coupled through an automated N-storm module, and four IXON Ultra897 EMCCD Cameras (Andor). For dSTORM imaging, the automated objective collar and the hardware auto-focus were activated. The 647 nm laser was set to a power of 100 % and images were acquired at 80 ms integration time for at least 15000 frames or until blinking events were negligible.

Sensor calibration

Epac1-camps-based cAMP FRET sensors were calibrated using a saponin permeabilization approach. First, the intracellular pH of HEK cells was assessed as described before (Koschinski and Zaccolo, 2015). Resulting pH value of 7.5 was used in all subsequent steps for intracellular buffers. Subsequently, the right combination of a KCl- and K-glutamate-based intracellular buffer was assessed in CHO cells resulting in a combination of 45% KCl- + 55% K-glutamate-based buffer, used during all calibration experiments. KCl- and K-glutamate based buffers contained 135 mM KCl/135 mM K-glutamate x H₂O, 10 mM NaCl, 6.49 mM MgCl₂ x 6H₂O, 0.00073 mM CaCl₂ x 2H₂O, 0.5 mM EGTA, 10 mM HEPES (pH=7.5). For calibration, HEK cells were maintained in intracellular buffer at room temperature, 10-12 μg/mL saponin was added to permeabilize the cells, together with a defined concentration of cAMP (range 0-1 mM, one concentration per cover slip).

cAMP ELISA

48 h after transfection, HEK cells were washed once with FRET buffer and incubated at 37°C for 25 min with GLP-1 + 100 μM IBMX (for the concentration response curve), 10 μM Fsk+100 μM IBMX (positive control), 100 μM IBMX (negative control). After incubation, buffer was aspirated and 260 μL of 0.1 M HCl were added to lyse the cells. Cells were incubated for 20 min at room temperature and then scraped off the surface. Lysates were centrifuged at 1000 x g for 10 min and the supernatants were diluted 1:10 before proceeding with the ELISA assay. ELISA (cyclic AMP ELISA Kit, Cayman chemicals, Michigan, USA) was conducted in a 96-well microtiter format as follows: 50 μL of the diluted cell supernatants were added to each well (duplicates). To each well, 50 μL cAMP AChE tracer and 50 μL cAMP ELISA antiserum were added. The plate was sealed and incubated at 4°C for 18 h. Cells were rinsed 5 times with wash buffer and 200 μL of freshly reconstituted Ellman's reagent was added to each well. The plate was covered with aluminum foil and let develop on an orbital shaker for 90 min at room temperature and absorbance was read at 405 nm in a Synergy Neo2 plate reader (BioTek, Vermont, USA).

cAMP accumulation assays by HTRF

HEK cells, transfected with GLP-1R biosensors were washed 48 h after the transfection, trypsinized, resuspended in 1x stimulation buffer and seeded at a density of 800 cells per well into white 96-well low-volume plates (Cisbio). Cells were incubated for 30 min at 37 °C with a concentration range of GLP-1 diluted in 1x stimulation buffer supplemented with 200 μM IBMX (5x stimulation buffer 1 from the cAMP Gs dynamic kit HTRF (Cisbio) was diluted to 1x with ddH₂O, supplemented with 0.2 % BSA (VWR International GmbH), and sterile filtered (pH=7.4)). cAMP accumulation was measured in a 96-well low volume microtiter plate (Cisbio) using the cAMP Gs dynamic kit HTRF (Cisbio). To do so, 5 μL cAMP-d2 dilution was added to each well, followed by 5 μL anti-cAMP-cryptate dilution. The microtiter was incubated at the room temperature for 1 h before the measurement.

CHO cells, transfected with β₂-AR biosensors were washed 24 h after the transfection, trypsinized, resuspended in 1x stimulation buffer and seeded at a density of 4000 cells per well into white 96-well low-volume plates (Cisbio). Cells were incubated for 30 min at 37 °C with a concentration range of isoproterenol diluted in 1x stimulation buffer supplemented with 200 μM IBMX. cAMP accumulation was measured using the cAMP Gs HiRange kit HTRF (Cisbio) as stated above. Plate reader experiments were conducted using a Synergy Neo2 plate reader (BioTek, Vermont, USA), equipped with HTRF filter optics (excitation filter 330/80 nm; dual emission filter: 662/10 nm - 665/8 nm). Concentration–effect curves were fitted by a three-parameter logistic function yielding parameter values for a ligand's potency (pEC₅₀).

Forskolin-induced PKA phosphorylation

HEK cells, expressing AKAR4 biosensors were washed 24 h after the transfection, trypsinized, resuspended and transferred to Poly-D-Lysine-precoated black-wall, black-bottomed 96-well plates (Brand) at a density of 60,000 cells/well. On the next day, cells were washed and medium was replaced with 90 μL FRET buffer. Basal FRET ratio was read for 5 min and subsequently, 10 μL of 10x forskolin dilutions or FRET buffer (negative control) was applied to each well and the FRET ratio was recorded for 20 min. Plate reader experiments were conducted at 37 °C using a Synergy Neo2 plate reader (BioTek, Vermont, USA), equipped with filter optics (excitation filter 420/50 nm; dual emission filter: 485/20 nm - 540/25 nm). FRET ratios were defined as corrected acceptor emission/donor emission. FRET ratios before ligand/buffer addition were averaged and defined as FRET_{basal}. To quantify ligand-induced FRET changes, ΔFRET was calculated for each well and time point as percent over basal ($[(\text{FRET}_{\text{stim}} - \text{FRET}_{\text{basal}}) / \text{FRET}_{\text{basal}}] \times 100$). Subsequently, the average ΔFRET of buffer-treated control wells was subtracted (Schihada et al., 2021). Concentration–effect curves were fitted by a three-parameter logistic function yielding parameter values for a ligand's potency (pEC₅₀).

Quantitative analysis of cAMP gradients at the nanometer scale

In our quantitative considerations (Methods S1) we assume a cytosolic PDE concentration of 3 nM and a cAMP diffusion coefficient of $D = 100 \mu\text{m}^2/\text{s}$ (Bock et al., 2020). Based on this, a constant that describes the decrease of $[\Delta\text{cAMP}]$ with increasing distance from the

source in stationary profiles by cytosolic PDEs is given by $0.17 \mu\text{m}^{-1}$ (Methods S1). Thus, we can neglect cAMP degradation by cytosolic PDEs on the lengthscale of 60 nm.

To quantify how cAMP concentrations at GPCRs decrease over a nanometer range, the [cAMP] values (Figure 7B) at GLP-1R and the cytosol were fit to the corresponding solution of the diffusion equation (Methods S1)

$$[\text{cAMP}] = 2A/r + B, \quad (\text{Equation 1})$$

where r denotes the cAMP distance from the receptor, A denotes the cAMP concentration increase above bulk at 2 nm distance from the receptor, and B signifies the cAMP concentration in the cytosol that was constrained to the cytosolic [cAMP] (150 nM).

QUANTIFICATION AND STATISTICAL ANALYSIS

Confocal images were analyzed using ImageJ. Each image was corrected by subtracting the average background fluorescence. Contrast was enhanced while keeping the saturated pixels at 0.1%. dSTORM movies were processed and analyzed in ImageJ using the Thunderstorm plugin (Ovesny et al., 2014; Schneider et al., 2012).

Statistical analyses and curve fitting were performed with Prism 7.0 (or newer) software (GraphPad Software, San Diego, USA) and OriginPro (OriginLab Corporation, Northampton, USA). Normalized FRET ratios are expressed as the mean \pm SEM (ΔFRET (%max)). In single cell experiments, all cells were analyzed individually and plotted as symbols in all bar graphs. For normalization of FRET ratios (and plotting of these values in bar graphs), we used the plateaus of the trace that were reached after ligand additions. We refer to the number of individual cells analyzed as n -number, and this n -number was used for statistical analysis. All data were tested for Gaussian distribution using the D'Agostino-Pearson normality test. Differences between means were assessed by a two-tailed Student's t -test (for two groups) or a one-way analysis of variance (ANOVA, for three or more groups) followed by Tukey's post hoc test for normally distributed data and a Kruskal-Wallis test in the case of non-normally distributed data. Differences were considered significant for values of $p < 0.05$. P values > 0.05 are indicated in the figures as not significantly different (ns). All experiments and representative data shown were repeated at least three times and performed with independent samples. Statistical details of all experiments can be found in the figures and figure legends.

Supplemental figures

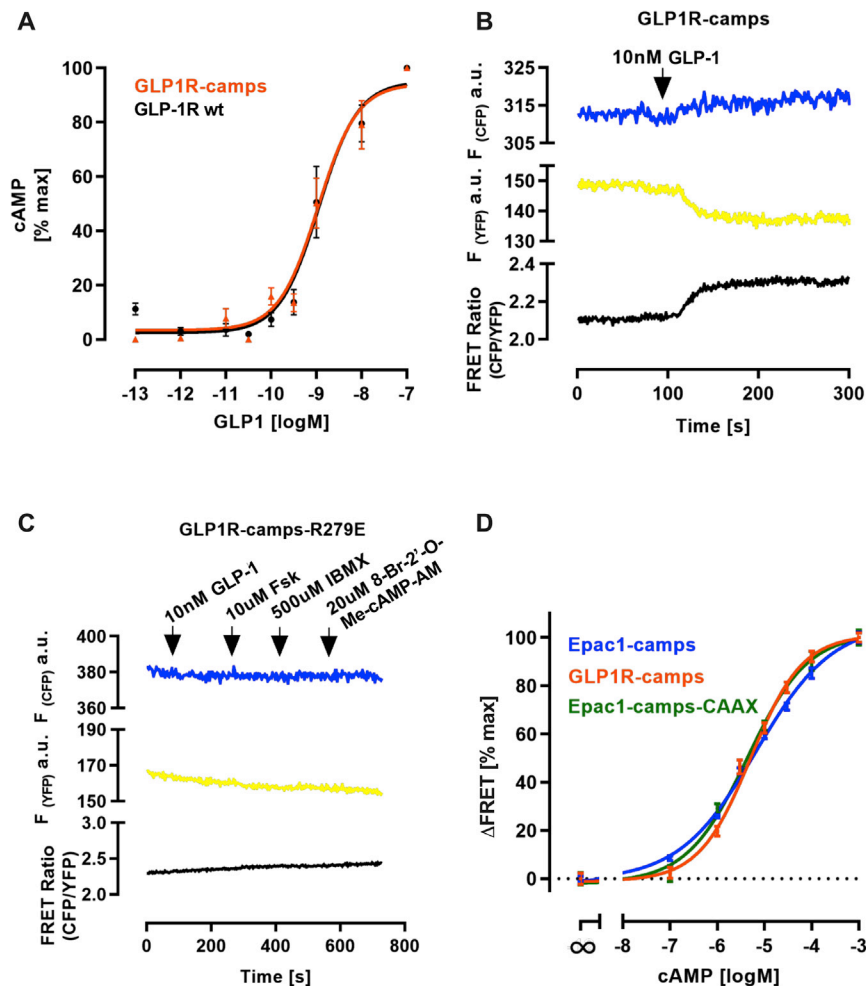


Figure S1. *GLP1R-camps* is a functional GPCR for cAMP sensing, related to Figure 1

(A) *GLP1R-camps* is a bona fide GPCR that is not compromised with regard to GLP-stimulated whole-cell cAMP production. Shown are concentration-response curves of GLP-1-induced whole-cell cAMP production (measured by ELISA) for *GLP1R-camps* (orange) in comparison with GLP-1R WT (black). Data were normalized to saturating GLP-1 concentrations and fitted to a three-parameter logistic function yielding similar potencies (pEC_{50}) for GLP-1 at *GLP1R-camps* (9.02 ± 0.11) and GLP-1R WT (8.99 ± 0.10). Data are means \pm SEM from three independent experimental days for each construct.

(B) Fluorescence intensity traces of CFP and YFP and resulting FRET ratio (CFP/YFP) recorded in HEK cells transiently expressing *GLP1R-camps*. 10 nM GLP-1 stimulation induces an increase in the CFP and a decrease in the YFP channel, respectively, confirming agonist-induced FRET changes. Traces are representative for 10 cells from five independent experiments.

(C) Fluorescence intensity traces of CFP and YFP and resulting FRET ratio (CFP/YFP) were recorded in HEK cells expressing the cAMP binding-deficient *Epac1-camps* mutant R279E fused to the GLP-1R. No changes in fluorescence intensities or FRET ratio are observed upon stimulation with various compounds that lead to cAMP production (indicated in the figure), or the *Epac*-specific cAMP analog 8-Br-2'-O-Me-cAMP-AM. Traces are representative for 10 cells from four independent experiments.

(D) Attaching *Epac1-camps* to GLP-1 receptors (*GLP1R-camps*) or targeting it to the membrane (*Epac1-camps-CAAX*) does not impair binding of cAMP. Shown are concentration-response curves generated using HEK cells expressing cytosolic *Epac1-camps* (blue), *GLP1R-camps* (orange), or *Epac1-camps-CAAX* (green) upon addition with the indicated cAMP concentrations in the presence of saponin (12 μ g/mL). Data are normalized to baseline (no cAMP, set to 0%) and maximal stimulation upon 1 mM cAMP addition (set to 100%). pEC_{50} (mean \pm SEM) *Epac1-camps* = 5.18 ± 0.05 , *GLP1R-camps* = 5.29 ± 0.05 , and *Epac1-camps-CAAX* = 5.36 ± 0.09 . Data are means \pm SEM of 6 independent experimental days for each construct.

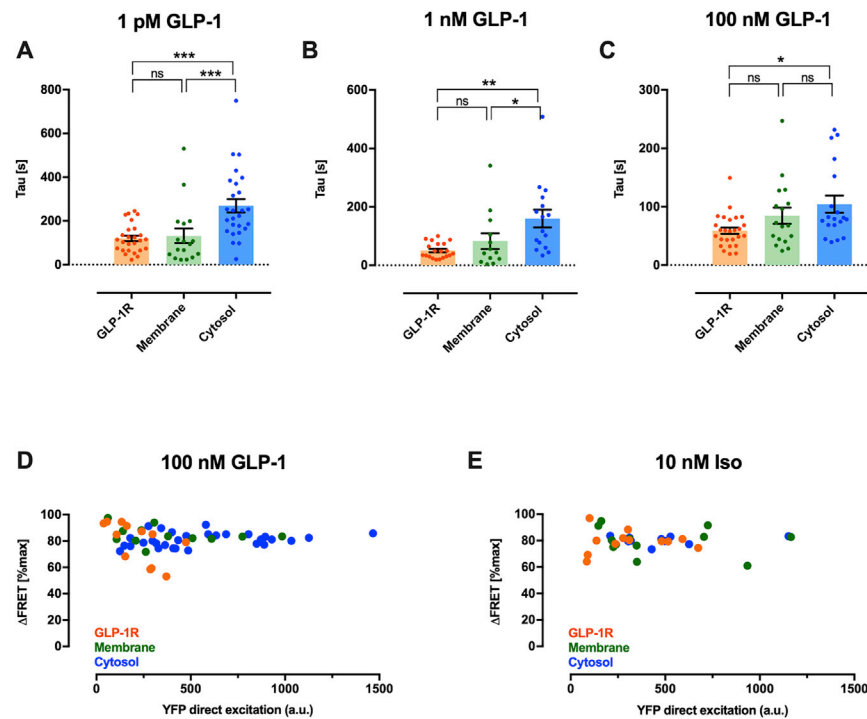


Figure S2. Apparent kinetic constants of GLP-1-induced FRET changes and expression levels of biosensors, related to Figure 2

(A–C) Apparent kinetic constants (Tau) of FRET changes induced by stimulation with 1 pM (A), 1 nM (B), or 100 nM (C) GLP-1 for the GLP-1R (orange), membrane (green), and cytosolic compartment (blue). GLP-1 was added to the bath and, upon signal onset, FRET traces were fitted to a one-phase exponential association function yielding the indicated kinetic constants. (A) $n = 26$ (*GLP1R-camps*), $n = 17$ (*Epac1-camps-CAAX*), and $n = 26$ (*Epac1-camps*) cells from 5, 3, and 3 independent experiments, respectively.

(B) $n = 20$ (*GLP1R-camps*), $n = 13$ (*Epac1-camps-CAAX*), $n = 16$ (*Epac1-camps*) cells from 4, 7, and 5 independent experiments, respectively.

(C) $n = 26$ (*GLP1R-camps*), $n = 17$ (*Epac1-camps-CAAX*), and $n = 19$ (*Epac1-camps*) cells from 5, 6, and 7 independent experiments, respectively. The columns represent means, the vertical bars SEM, *** $p < 0.001$, ** $p < 0.01$, * $p < 0.05$ according to a Kruskal-Wallis test; ns, not significantly different.

(D and E) Ligand-induced FRET responses are independent of expression level of biosensors. Shown are corrected and normalized FRET ratios induced by the indicated GLP-1 (D) or Iso (E) concentration. HEK cells were transiently transfected with *GLP1R-camps* (GLP-1R, orange), *GLP1R-IRES2-Epac1-camps-CAAX* (membrane, green), and *GLP1R-IRES2-Epac1-camps* (cytosol, blue). FRET ratios are normalized to baseline (set to 0%) and maximal stimulation upon FSK (10 μ M)/IBMX (100 μ M) treatment (set to 100%).

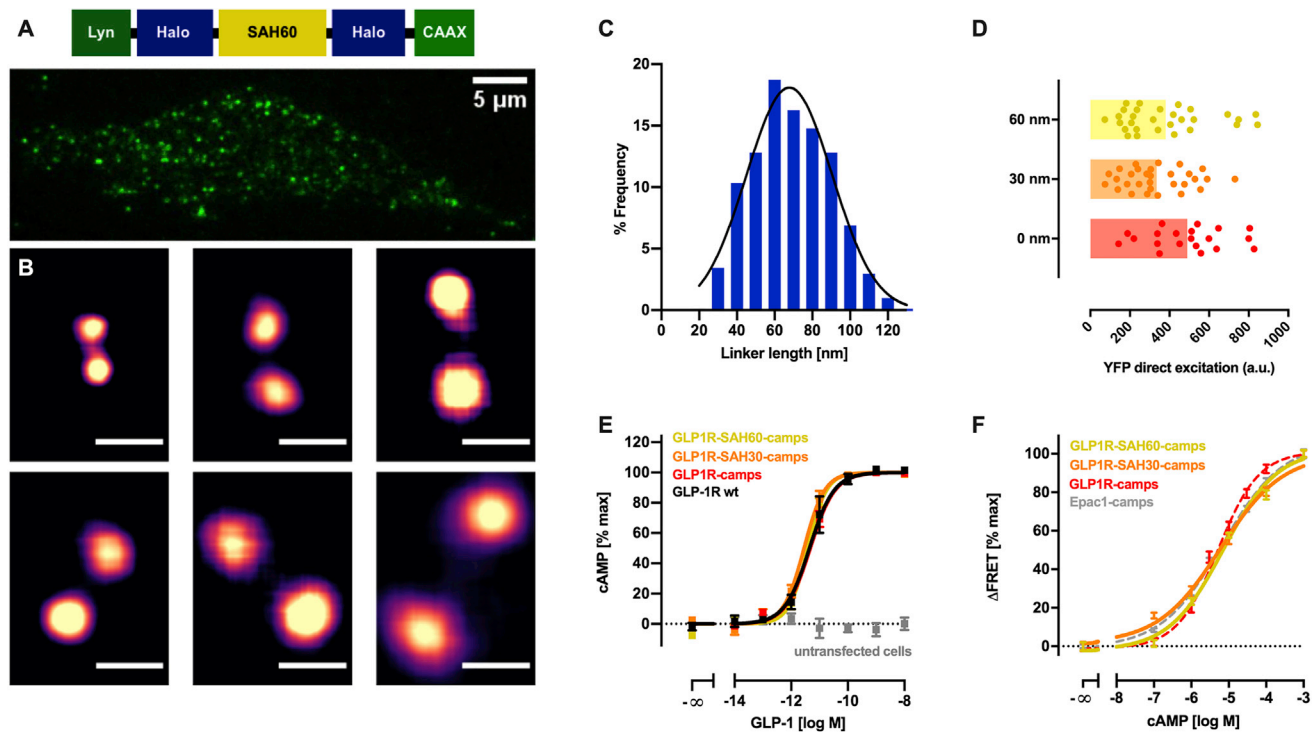


Figure S3. Characterization of GPCR nanorulers, related to Figure 3

(A) Top: domain structure of the SAH60 linker construct flanked by two HaloTags, targeted to the cell membrane to perform dSTORM imaging. Bottom: representative first frame from the localization microscopy stacks of a CHO cell expressing the indicated construct labeled with Halo JF-646, from which the reconstructed super-resolution image was generated.

(B) Closeup view of representative linkers containing two Halo JF-646 fluorophores. Scale bar, 60 nm.

(C) Histogram depicting the frequency distribution of linker length. Average length is 68.8 ± 1.42 nm. Peak abundance in the histogram is at 60 nm. Data represent mean \pm SEM of 203 linkers measured from 10 different cells.

(D) Expression levels of all GPCR nanorulers are similar. Shown are YFP emission values (a.u.) of HEK cells transiently transfected with *GLP1R-camps* (0 nm, red), *GLP1R-SAH30-camps* (30 nm, orange), and *GLP1R-SAH60-camps* (60 nm, yellow).

(E) *GLP1R-SAH30-camps* and *GLP1R-SAH60-camps* are bona fide GPCRs that are not compromised with regard to GLP-1-stimulated whole-cell cAMP production. Shown are concentration-response curves of GLP-1-induced whole-cell cAMP production (measured by HTRF, STAR Methods) for *GLP1R-SAH60-camps* (yellow), *GLP1R-SAH30-camps* (orange), and *GLP1R-camps* (red) in comparison with GLP-1R WT (black) and untransfected HEK cells. Data were normalized to saturating GLP-1 concentrations and fitted to a three-parameter logistic function yielding similar potencies (pEC_{50}) for GLP-1 at *GLP1R-SAH60-camps* (11.4 ± 0.10), *GLP1R-SAH30-camps* (11.6 ± 0.10), *GLP1R-camps* (11.3 ± 0.10), and GLP-1R WT (11.3 ± 0.20). Data are means \pm SEM from three to four independent experimental days for each construct.

(F) GPCR nanorulers are not impaired in their affinities for cAMP. Shown are concentration-response curves generated using HEK cells expressing *GLP1R-SAH30-camps* (orange) and *GLP1R-SAH60-camps* (yellow) upon addition of the indicated cAMP concentrations in the presence of saponin (12 μ g/mL). Data are normalized to baseline (no cAMP, set to 0%) and maximal stimulation upon 1 mM cAMP addition (set to 100%). pEC_{50} (mean \pm SEM) *GLP1R-SAH30-camps* = 5.23 ± 0.07 , *GLP1R-SAH60-camps* = 5.15 ± 0.07 . Data are means \pm SEM of 6 and 7 individual experimental days, respectively. *GLP1R-camps* (red) and *Epac1-camps* (gray) are re-plotted as dashed lines from Figure S1 for comparison. One-way analysis of variance (ANOVA) with Tukey's post hoc test of all pEC_{50} values (*Epac1-camps*, *GLP1R-camps*, *GLP1R-SAH30-camps*, and *GLP1R-SAH60-camps*) shows no significant difference, $p > 0.05$.

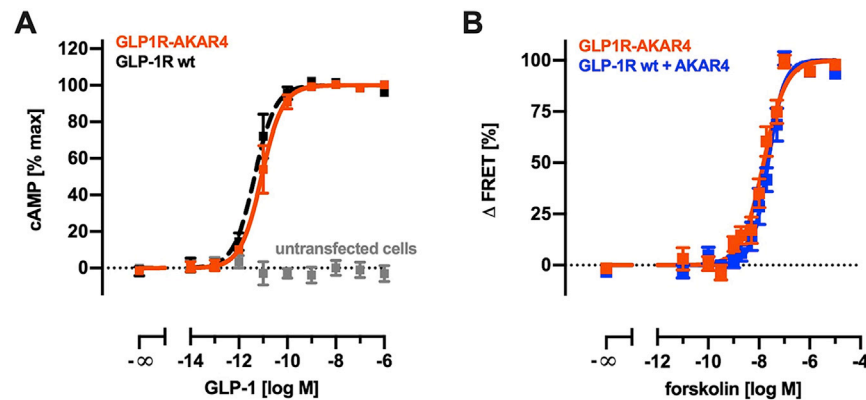


Figure S4. *GLP1R-AKAR4* is functional with regard to cAMP signaling and to PKA phosphorylation sensitivity, related to Figure 5

(A) *GLP1R-AKAR4* is a bona fide GPCR that is not compromised with regard to GLP-1-stimulated whole-cell cAMP production. Shown are concentration-response curves of GLP-1-induced whole-cell cAMP production (measured by HTRF, [STAR Methods](#)) for *GLP1R-AKAR4* (orange) in comparison with GLP-1R WT (black), and untransfected HEK cells (gray). Data were normalized to saturating GLP-1 concentrations and fitted to a three-parameter logistic function yielding similar potencies (pEC_{50}) for GLP-1 at *GLP1R-AKAR4* (11.0 ± 0.20) and GLP-1R WT (11.3 ± 0.20). Data are means \pm SEM from 4 independent experimental days for each construct. Data for GLP-1R WT are re-plotted from [Figure S3](#).

(B) Tethering *AKAR4* to GLP-1 receptors (*GLP1R-AKAR4*, orange) does not change its phosphorylation sensitivity. Shown are concentration-response curves of forskolin-induced whole-cell PKA activity that is sensed by *AKAR4* (blue) and *GLP1R-AKAR4* (orange) and detected as an increase in FRET ([STAR Methods](#)). Data were normalized to saturating forskolin concentrations and fitted to a three-parameter logistic function yielding similar potencies (pEC_{50}) for forskolin at *GLP1R-AKAR4* (7.82 ± 0.05) and *AKAR4* (7.65 ± 0.05). Data are means \pm SEM from 5 independent experimental days for each construct.

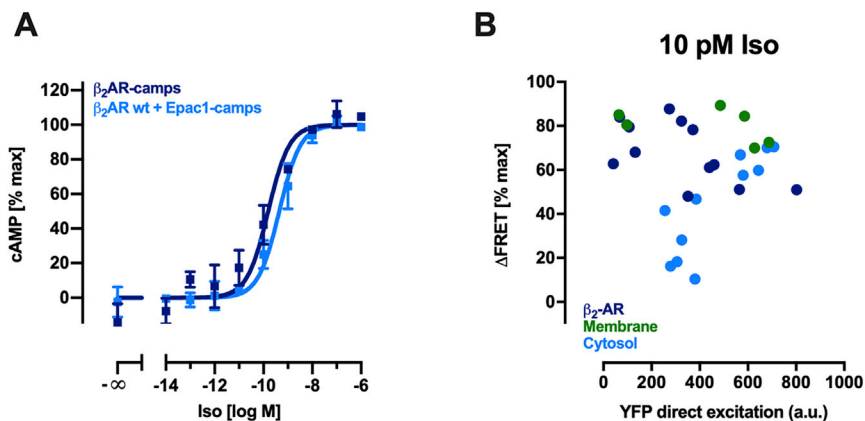


Figure S5. Expression and functional validation of β_2AR -camps, related to Figure 6

(A) β_2AR -camps is a bona fide GPCR that is not compromised with regard to Iso-stimulated whole-cell cAMP production. Shown are concentration-response curves of Iso-induced whole-cell cAMP production (measured by HTRF, STAR Methods) for β_2AR -camps (dark blue) in comparison with β_2 -AR WT (light blue). Data were normalized to saturating Iso concentrations and fitted to a three-parameter logistic function yielding similar potencies (pEC_{50}) for Iso at β_2AR -camps (9.87 ± 0.28) and β_2 -AR WT (9.37 ± 0.29). Data are means \pm SEM from 3 independent experimental days for each construct.

(B) Iso-induced FRET responses are independent of the expression level of biosensors. Shown are corrected and normalized FRET ratios induced by 10 pM Iso. HEK-AD cells were transiently transfected with β_2AR -camps (β_2AR , dark blue), β_2AR -IRES2-Epac1-camps-CAAX (membrane, green), and β_2AR -IRES2-Epac1-camps (cytosol, light blue). FRET ratios are normalized to baseline (set to 0%) and maximal stimulation upon FSK (10 μ M)/IBMX (100 μ M) treatment (set to 100%).